Available online at www.sciencedirect.com
SCIENCE DIRECT®
Journal of Sound and Vibration 291 (2006) 323–348
JOURNAL OF SOUND AND VIBRATION
www.elsevier.com/locate/jsvi

Replacement of a summation by an integration in structural acoustics

G. Maidanik*, K.J. Becker, L.J. Maga

Department of the Navy, Naval Surface Warfare Center, Carderock Division, David Taylor Model Basin, Code 7030, 9500 MacArthur Building, West Bethesda, MD 20817-5700, USA

Received 8 October 2004; received in revised form 17 May 2005; accepted 13 June 2005
Available online 24 August 2005

Abstract

An analytical formulation of a transfer function pertaining to a simple structural model is used both to examine the result of replacing a summation by an integration and to interpret this result. The model consists of a coated plate immersed in fluid media on either side. The first fluid interfaces the coating atop and is semi-infinite in extent. The second fluid interfaces the bottom of the plate and terminates at a baffle that defines a reflection coefficient. An external drive is placed on a plane that lies in the fluid between the plate and the baffle. Focus is centered on the transfer function between a spectral component in the external drive and a spectral component on the interface with the top fluid. The presence of the baffle generates resonances and anti-resonances in this transfer function. These are discernible in those regions of the frequency domain in which the modal overlap parameters are less than unity. In those regions of the frequency domain in which the modal overlap parameters approach and exceed unity the resonances and the anti-resonances merge into values that are the same as those in the absence of the cavity. It transpires that replacing a summation by an integration is tantamount to artificially merging the resonances and the anti-resonances also in those regions in which the modal overlap parameters are less than unity. The merging, again, are into values that are the same as those in the absence of the cavity. It follows then that in those regions of the frequency domain where resonances and anti-resonances are present under summations, these resonances and anti-resonances are suppressed when the summations are replaced by integrations.

*Corresponding author.
E-mail address: maidanikg@nswccd.navy.mil (G. Maidanik).

0022-460X/$ - see front matter © 2005 Elsevier Ltd. All rights reserved.
doi:10.1016/j.jsv.2005.06.015

1. Introduction

An estimate of the response of a resonant *complex* dynamic system carries terms and factors that involve summations that generate the resonances and the anti-resonances. Approximations for the estimate are often made by converting the summations to corresponding integrations [1–6]. One might ask: What is the criterion that legitimizes this conversion? An answer to this question is briefly sought and exemplified in this paper.

In Section 2, the complex dynamic system having transfer functions in which *resonances* and *anti-resonances* are manifested, is described and defined. The formalism focuses on the transfer of spectral components in the external drive to spectral components that emerge on the interface of a coated plate with the top fluid (cf. Fig. 1). The top fluid occupies the semi-infinite space above that interface. The external drive is placed on a plane parallel to the plate in the bottom fluid a specific distance below the plate. Since there are no discontinuities, either in the plate or in the coating and since these elements of the structure are assumed to be isotropic, the transfer is one-to-one. A spectral component in the external drive is spectrally duplicated in the component that emerges on the interface with the top fluid. The spectral component that is selected for investigation in this paper is supersonic. To render in this transfer function resonances and anti-resonances a baffle is placed in the bottom fluid on a parallel plane to the plate. The baffle is uniform and it lies below the plane in which the external drive resides. Assisted by Fig. 1, the analytical expressions for the transfer function are derived. Fig. 1a depicts the elements of the model. The physical construction of the model is shown in Fig. 1b. An equivalent circuit diagram of the model is presented in Fig. 1c. A brief synopsis of the analysis, as deduced from Fig. 1c, is given in Table 1. The transfer function (T_{bc}), in the presence of both the cavity and the coating, is derived first. The presence of the cavity is designated by the subscript (b) and that of the coating by the subscript (c). The reductions in the expression for the transfer function (T_{bc}) to (T_c) when the cavity is removed, to (T_b) when the coating is removed and to (T) when the cavity as well as the coating are removed, are derived successively.

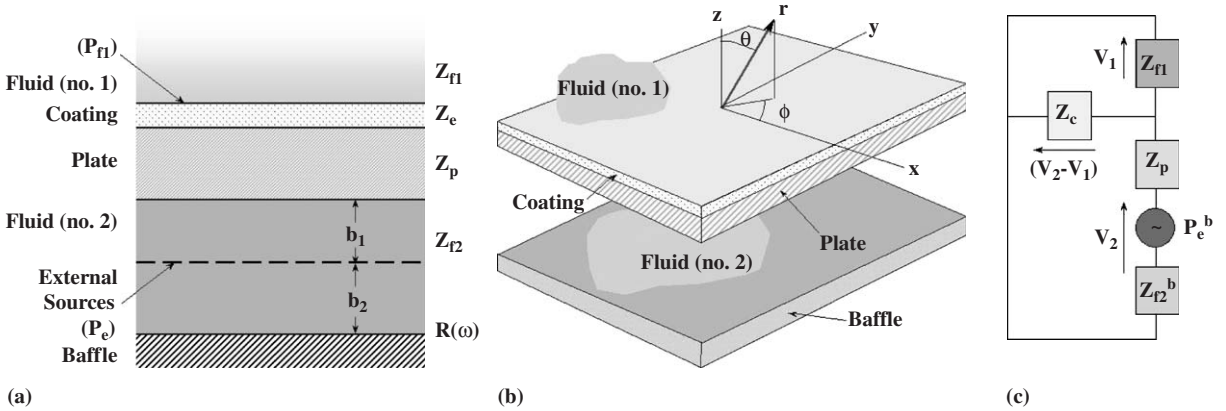

Fig. 1. (a) Elements of the model; (b) physical construction of the model; (c) equivalent circuit diagram for the model.

Table 1
A brief synopsis of the analysis of the model depicted in Fig. 1

$$Z^b V = P_e^b$$
$$V = \{V_1, V_2\}$$
$$P_e^b = \{O, P_e^b\}$$
$$P_e^b = \{C, P_e\}$$
$$Z^b = \begin{pmatrix} (Z_{f1} + Z_c) & -Z_c \\ -Z_c & (Z_c + Z_p + Z_{f2}^b) \end{pmatrix}$$
$$Z_{f2}^b = (Z_{f2} A)$$
$$P_{f1} = (Z_{f1} V_1)$$

In Section 3, computations pertaining to the transfer functions $(T_{bc}), (T_c), (T_b)$ and (T), as functions of an appropriately normalized frequency, are carried out. As expected, resonances and anti-resonances are found only in the results of computations involving (T_{bc}) and (T_b) for these are the only transfer functions governed by the presence of the cavity. Again, as expected, the results of computations involving (T_c) and (T), for which the cavity is absent, are devoid of resonances and anti-resonances. In this paper the results of the computations are presented in a set of three graphs. In the first graph the modulus of (T_{bc}) is depicted by a solid curve and the modulus of (T_c) is depicted by a dotted curve; e.g., in Fig. 2a. In the second graph the modulus of (T_b) is depicted by a solid curve and the modulus of (T) is depicted by a dotted curve; e.g., in Fig. 2b. Each of these two graphs contrast the transfer function in the presence of the cavity (solid curves) with the corresponding transfer function in the absence of the cavity (dotted curves). In the third graph the modulus of (T_{bc}/T_b) is depicted by a solid curve and the modulus of (T_c/T) is depicted by a dotted curve; e.g., in Fig. 2c. This third graph exhibits and contrasts the influence of the coating on the transfer function in the presence of the cavity (solid curve) with the transfer function in the absence of the cavity (dotted curve). The influence on the transfer functions of *damping* in the cavity is also computed and investigated. Both, the volume (bulk) damping and the damping resulting from the absorption in the surface of the baffle, are considered.

Most previous works on this subject focused on deriving an *induced loss factor* resulting from the coupling of *a master dynamic* system; e.g., a harmonic oscillator, to *an adjunct dynamic* system; e.g., a set of harmonic oscillators [1–6]. The induced loss factor is the apparent increase in the loss factor that is experienced by the master dynamic system due to this coupling [1–8]. In this paper the damping is defined in terms of modal overlap parameters rather than merely in terms of loss factors. In particular, the focus is on the property that in a region in the frequency domain in which resonances and anti-resonances prevail, the modal overlap parameter is less than unity, whereas in a region of the frequency domain that is characterized by a modal overlap parameter that exceeds unity, the resonances and anti-resonances are suppressed [9,10]. The suppression is a convergence of peaks in the resonances and of nadirs in the anti-resonances onto values that are commensurate with modal overlap parameters that exceed unity. Thus, although the modal overlap parameter is equal to the product of the frequency, the loss factor and the modal density, in the consideration of the replacement of a summation by an integration the individual values of these constituent factors is moot. The value of their product, which is the modal overlap parameter, plays the only significant role [9,10].

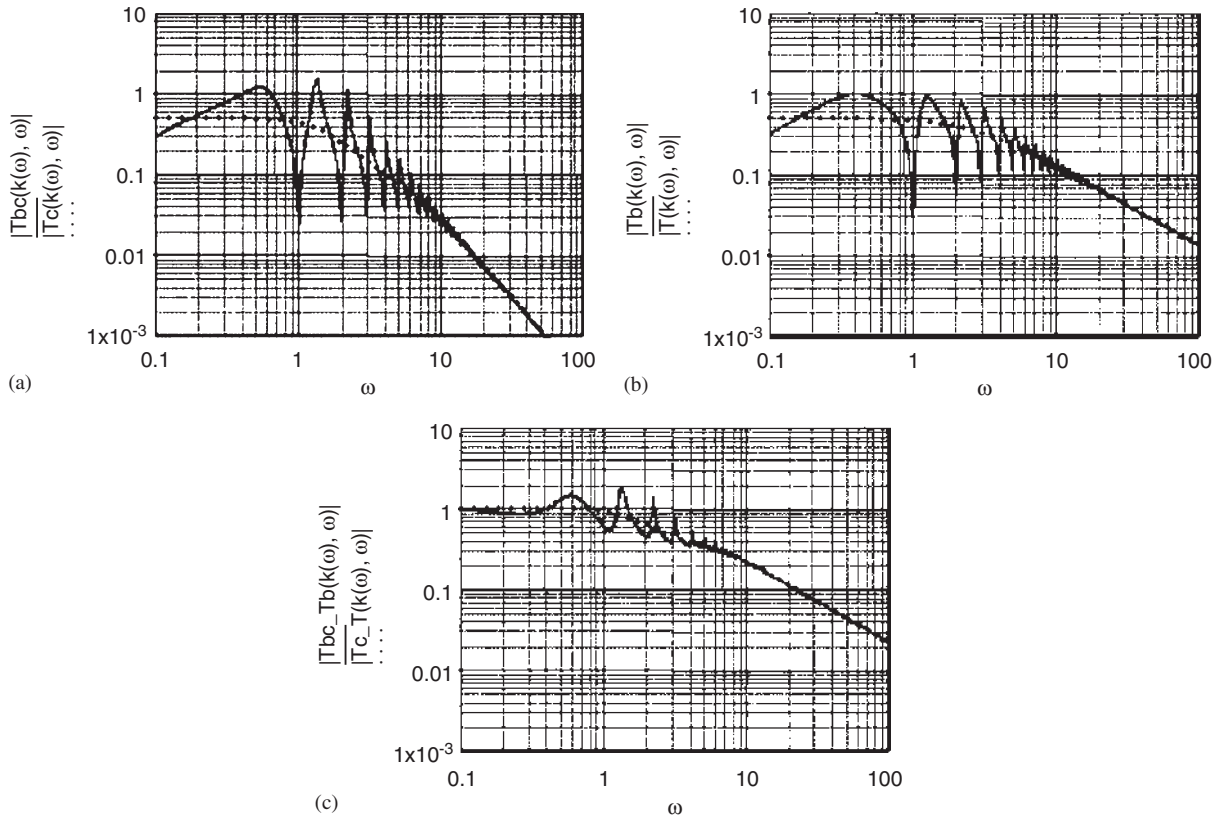

Fig. 2. (a) The transfer function, as a function of the normalized frequency (ω), for standard coated plate under the standard condition $|R(\omega)| = \exp(-10^{-3})$, $\eta = 10^{-2}$, $\eta_c = 10^{-2}$, $s = 1$ $(\omega_c) = 10$, $(b) = \pi$, $(b_1) = 0$, $(k) = 0$, fluid loading factor $\gamma = (\rho_1 c_1/\omega_o m\omega_c) = 0.13$ and the fluids on both sides, fluid no. 1 and fluid no. 2, possess equal properties; i.e., $\rho_1 = \rho_2$ and $c_1 = c_2$. Note that frequencies and time scales are normalized by (ω_o) and wavenumbers and spatial separations are normalized by (ω_o/c_1). (b) As in Fig. 2(a) except that the plate is uncoated. (c) The ratio of the transfer functions, as a function of the normalized frequency (ω). The ratio is between the coated and uncoated plates; i.e., Fig. 2(a) divided by Fig. 2(b).

In Section 4, summations in the expressions for the transfer functions, under several varying conditions of damping, are converted to corresponding integrations. The results of computations show that the resonances and the anti-resonances, that exist when the summations prevail, are suppressed when these summations are converted to the corresponding integrations. It is interpreted that in those regions of the frequency domain in which the modal overlap parameters are less than unity, the conversion of the summations to integrations is tantamount to inducing artificially these modal overlap parameters to exceed unity. One recalls that in a region where the modal overlap parameters are less than unity, the footprints of the resonances and the anti-resonances are clearly discernible. Thus, the conversion of the summations to the corresponding integrations suppresses the modal character of the transfer functions investigated here. The suppression is such as to validate the ''mean-value method'' proposed by Skudrzyk [11].

Finally, a number of variations on the theme are covered in Appendix B. These are presented under a separate cover in order not to clutter the main theme of the paper. That theme is to decipher the procedures and the meanings that encompass the conversion of summations to integrations in structural acoustics. It is hoped that this limited theme is adequately illustrated and that the arguments are convincing enough.

2. Derivation of the expressions for the transfer function

The derivation is performed on the dynamic system shown in Fig. 1. This dynamic system is composed basically of a plate immersed, on each side, by a fluid; fluid no. 1 atop and fluid no. 2 below. The plate is backed by a baffle. The baffle is uniform and is placed on a plane a normalized distance (b) below the plate; $b = (b_1 + b_2)$; $(b_1) < (b)$. The normalized distances (b_1) and (b_2) are yet to be defined. All distances; e.g., b, b_1 and b_2, are normalized by (c_1/ω_o), where (c_1) is the speed of sound in the top fluid (fluid no. 1) and (ω_o) is the resonance frequency of the oscillator formed by the surface stiffness (K_c) of the coating, and the surface mass (m) of the plate; $(\omega_o)^2 = (K_c/m)$. In this paper (ω_o) is used as a normalizing factor for all other frequencies; e.g., (ω) designates the so normalized frequency variable. Also in this paper all wavenumbers are normalized by the factor (ω_o/c_1); e.g., (k) designates the so normalized wavenumber variable. A thin slab of compliant coating is attached to the top side of the plate, the other side of the coating interfaces the fluid atop (fluid no. 1) as depicted in Figs. 1a and b. A set of external drives are distributed on a plane a normalized distance (b_1) below the plane of the plate and a normalized distance (b_2) above the baffle as indicated in Fig. 1a. The transfer function $T_{bc}(\mathbf{k}, \omega)$, relating the spectral component $P_e(\mathbf{k}, \omega)$, in the external drive, to the spectral component $P_{f1}(\mathbf{k}, \omega)$, in the pressure on the interface with the semi-infinite fluid atop (fluid no. 1), is of special interest in this paper. [The subscript $(f1)$; i.e., as in (P_{f1}), indicates that this quantity is ascertained in fluid no. 1.] The normalized vector $\{\mathbf{k}, \omega\}$ is a spectral variable, where $(\mathbf{k})$ is the normalized wavevector in the plane of the plate and (ω) is the normalized frequency. The analytical derivation of this transfer function is assisted by Fig. 1c and Table 1. In this vein one may derive the transfer function $T_{bc}(\mathbf{k}, \omega)$ in the form

$$T_{bc}(\mathbf{k}, \omega) = [P_{f1}(\mathbf{k}, \omega)/P_e(\mathbf{k}, \omega)], \quad P_{f1}(\mathbf{k}, \omega) = [Z_{f1}(\mathbf{k}, \omega)V_1(\mathbf{k}, \omega)],$$

$$T_{bc}(\mathbf{k}, \omega) = Z(\mathbf{k}, \omega)G(\mathbf{k}, \omega)C(\mathbf{k}, \omega), \tag{1a}$$

where $V_1(\mathbf{k}, \omega)$ is the response of the interface of the coating with fluid no. 1, $Z(\mathbf{k}, \omega)$ is a parallel combination of the fluid surface impedance $Z_{f1}(\mathbf{k}, \omega)$ and the surface (stiffness) impedance $Z_c(\mathbf{k}, \omega)$ of the coating; namely

$$Z(\mathbf{k}, \omega) = Z_{f1}(\mathbf{k}, \omega)Z_c(\mathbf{k}, \omega)[Z_{f1}(\mathbf{k}, \omega) + Z_c(\mathbf{k}, \omega)]^{-1} \tag{2}$$

and $G(\mathbf{k}, \omega)$ is the surface admittance of the plate in situ

$$G(\mathbf{k}, \omega) = [Z(\mathbf{k}, \omega) + Z_p(\mathbf{k}, \omega) + Z^b_{f2}(\mathbf{k}, \omega)]^{-1}. \tag{3}$$

In Eqs. (1a), (2) and (3) the surface impedances are all normalized. The normalizing factor here is the imaginary part of the surface mass impedance; i.e., $[(m\omega_o)(\omega)]$, of the plate. Thus, for example,

the normalization of the surface impedance of the coating is

$$Z_c(\mathbf{k},\omega) = Z_c(\omega) = -i[K_c(1+\mathrm{i}\eta_c)/(m\omega_o^2)(\omega)^2] = -i(\omega)^{-2}(1+i\eta_c),$$

$$\omega_o^2 = (K_c/m) \tag{4}$$

and the normalization of the surface impedance of the top fluid (fluid no. 1) is

$$Z_{f1}(\mathbf{k},\omega) = Z_{f1}(k,\omega) = \gamma_1(\omega_c/\omega)[k_1(k,\omega)]^{-1}, \quad \gamma_1 = (\rho_1 c_1/\omega_o\omega_c m)$$

$$k_1(k,\omega) = (1-\alpha_1^2)^{1/2}U(1-\alpha_1^2) - i(\alpha_1^2-1)^{1/2}U(\alpha_1^2-1),$$

$$\alpha_1^2 = (k/\omega)^2, \quad |\mathbf{k}| = k, \tag{5a}$$

where (U) is the standard step function, $(\rho_1 c_1)$ is the characteristic impedance of fluid no. 1 and (ω_c) is the normalized critical frequency of the plate with respect to the top fluid (fluid no. 1). In this paper K_c is simply assumed to be a constant independent of $(\mathbf{k})$ and (ω). The normalized wavenumber $k_1(k,\omega)$ is the *viable* wavenumber in the top fluid (fluid no. 1) that describes, in that fluid, the propagation normal to the plane of the plate. As indicated in Eq. (5a) this wavenumber is dependent merely on (k) not on $(\mathbf{k})$ and, therefore, so is the normalized surface fluid impedance. The normalized fluid loading on the plate, due to the bottom fluid (fluid no. 2), is modified by the presence of the cavity in the manner

$$Z_{f2}^b(\mathbf{k},\omega) = Z_{f2}^b(k,\omega) = A(k,\omega)Z_{f2}(k,\omega), \tag{6}$$

where $Z_{f2}(k,\omega)$ is the normalized surface impedance of the bottom fluid in the absence of the cavity; namely

$$Z_{f2}(\mathbf{k},\omega) = Z_{f2}(k,\omega) = \gamma_2(\omega_c/\omega)[k_2(k,\omega)]^{-1}, \quad \gamma_2 = (\rho_2 c_2/\omega_o\omega_c m),$$

$$k_2(k,\omega) = (1-\alpha_2^2)^{1/2}U(1-\alpha_2^2) - i(\alpha_2^2-1)^{1/2}U(\alpha_2^2-1),$$

$$\alpha_2^2 = (c_2/c_1)^2\alpha_1^2, \quad |\mathbf{k}| = k. \tag{5b}$$

In Eq. (5b) $(\rho_2 c_2)$ is the characteristic impedance of fluid no. 2 and $k_2(k,\omega)$ is the normalized viable wavenumber that describes the propagation normal to the plane of the plate in the bottom fluid (fluid no. 2) [cf. Eq. (5b)]. The dimensionless factor $A(k,\omega)$ accounts for the modification, by the presence of the cavity, to the surface impedance of the bottom fluid (fluid no. 2). The expression for this factor may be derived by tracing the multiple reflections at the blocked plate and the surface of the cavity. The result is

$$Z_{f2}^b(k,\omega) = Z_{f2}(k,\omega)A(k,\omega), \quad A(\mathbf{k},\omega) = A(k,\omega),$$

$$A(k,\omega) = [1+R(\omega)\exp\{\mathrm{a}(k,\omega)\}][1-R(\omega)\exp\{\mathrm{a}(k,\omega)\}]^{-1},$$

$$\mathrm{a}(k,\omega) = \{-2i(c_1/c_2)(b\omega)k_2(k,\omega)\}(1-\mathrm{i}\eta), \tag{7a}$$

where (η) is the volume loss factor in the cavity, $\mathrm{a}(k,\omega)$ is the argument of the propagator in the bottom fluid from the plane of the plate to the surface of the baffle and back again, and $R(\omega)$ is the reflection coefficient on the surface of this baffle. Again, the reflection coefficient is assumed,

for simplicity sake, to be independent of the wavevector (**k**). There remains to define just another dimensionless factor; the $C(k,\omega)$ in Eq. (1). This dimensionless factor accounts for the modification to the external drive by the presence of the cavity. This factor accounts for any off-set of the external drive from the plane of the cavity before the multiple reflections in the cavity commence. This factor may be expressed in the form

$$P_e^b(\mathbf{k},\omega) = C(k,\omega)P_e(\mathbf{k},\omega),$$

$$C(k,\omega) = [1+(-1)^S R(\omega)\exp\{\mathrm{a}_1(k,\omega)\}][1-R(\omega)\exp\{\mathrm{a}(k,\omega)\}]^{-1},$$

$$\mathrm{a}_1(k,\omega) = \{-2i(c_1/c_2)[\omega(b-b_1)]k_2(k,\omega)\}(1-\mathrm{i}\eta), \tag{7b}$$

where $\mathrm{a}_1 \Rightarrow \mathrm{a}$ as $b_1 \Rightarrow 0$ and the index (s) designates the nature of the external drives; e.g., $s=0$ designates a monopole-like and $s=1$ designates a dipole-like external drive, [cf. Eq. (7a)]. Since there are no spatial-temporal discontinuities in the elements that compose the complex dynamic system, a spectral component in the external drive is spectrally duplicated in the component that emerges on the interface with the top fluid. This condition renders the normalized wavevector (**k**) a function of the normalized frequency; namely, $\mathbf{k}=\mathbf{k}(\omega)$. Moreover, if the spectral component that one seeks on the interface with the top fluid is to be supersonic, then $|\mathbf{k}(\omega)| = k(\omega) < \omega$. These conditions are incorporated in the formalism in this paper. In particular

$$k(\omega) = (\omega)\sin(\theta), \tag{8}$$

where the angle (θ) is the directional designation of a (supersonic) component on the interface with the top fluid (fluid no. 1). Finally, the normalized surface impedance of the plate is expressed in the form

$$Z_p(k,\omega) = i[(1-\mathrm{i}\eta_m) - (k^2/\omega\omega_c)^2(1+\mathrm{i}\eta_p)], \tag{9}$$

where the plate is assumed to be isotropic and (η_m) and (η_p) are, respectively, the mass-control and the stiffness-control loss factors in the plate and one is reminded, yet again, that (k), (ω_c) and (ω) are the normalized wavenumber, the normalized critical frequency and the normalized frequency, respectively. The normalizing factors are (ω_o/c_1), (ω_o) and (ω_o), respectively. Under all these assumptions and definitions, the transfer function $T_{bc}(\mathbf{k},\omega)$ is, in fact, isotropic

$$T_{bc}(\mathbf{k},\omega) \Rightarrow T_{bc}(k,\omega), \quad k = k(\omega) \tag{1b}$$

as can be readily verified reviewing Eqs. (1)–(9). A few asymptotic forms for Eq. (1) are useful. These are: The coating is removed by rendering $|Z_c|$ infinite; $|Z_c| \Rightarrow \infty$. In the absence of coating, Eq. (1) yields the transfer function $T_b(k,\omega)$ as

$$T_b(k,\omega) = Z_{f1}(k,\omega)G(k,\omega)C(k,\omega), \quad |Z_c| \Rightarrow \infty, \tag{10}$$

where the subscript (c) for the presence of the coating is removed and $G(k,\omega)$ is reduced to

$$G(k,\omega) \Rightarrow [Z_{f1}(k,\omega) + Z_p(k,\omega) + Z_{f2}^b(k,\omega)]^{-1} \tag{11}$$

[cf. Eqs. (2)–(9)]. The baffle may be removed by rendering the reflection coefficient $R(\omega)$, at the baffle interface with the bottom fluid (fluid no. 2), equal to zero; i.e., $R(\omega) \Rightarrow 0$. This removal renders $A(k,\omega)$ and $B(k,\omega)$ equal to unity. In the absence of the cavity; i.e., when $R(\omega) \Rightarrow 0$, but in the presence of the coating; i.e., when $|Z_c|(\omega) \nRightarrow \infty$, the transfer function $T_{bc}(k,\omega)$ stated in

Eq. (1) reduces to

$$T_c(k,\omega) = Z(k,\omega)G(k,\omega), \quad R(\omega) \Rightarrow 0, \text{ but } |Z_c| \nRightarrow \infty, \tag{12}$$

where the subscript (b) for the presence of the cavity is removed and $Z^b_{f2}(k,\omega)A(k,\omega)$ and $C(k,\omega)$ are reduced to

$$Z^b_{f2}(k,\omega) \Rightarrow Z_{f2}(k,\omega), \;\; A(k,\omega) = 1, \;\; C(k,\omega) \Rightarrow 1, \tag{13}$$

respectively, and the normalized admittance $G(k,\omega)$ is reduced to

$$G(k,\omega) = [Z(k,\omega) + Z_p(k,\omega) + Z_{f2}(k,\omega)]^{-1} \tag{14}$$

[cf. Eqs. (2)–(9)]. If, in addition to the removal of the cavity, the coating is also removed; i.e., $|Z_c| \Rightarrow \infty$, then the transfer function $T_c(k,\omega)$ further reduces from Eq. (12) to be

$$T(k,\omega) = Z_{f1}(k,\omega)G(k,\omega), \quad R(\omega) \Rightarrow 0 \quad \text{and} \quad |Z_c| \Rightarrow \infty, \tag{15}$$

where, the subscript (c) for the presence of the coating is removed by definition and $G(k,\omega)$ assumes the reduced form

$$G(k,\omega) \Rightarrow [Z_{f1}(k,\omega) + Z_p(k,\omega) + Z_{f2}(k,\omega)]^{-1} \tag{16}$$

[cf. Eqs. (2)–(9)]. One can define a simple coating such that (K_c) and (η_c) are constants, independent of the normalized frequency. Eqs. (1), (10), (12) and (15) can then be employed to compute the three pairs of quantities: $\{T_{bc}(k,\omega), T_c(k,\omega)\}, \{T_b(k,\omega), T(k,\omega)\}$ and $\{|T_{bc}(k,\omega)/T_b(k,\omega)|, |T_c(k,\omega)/T(k,\omega)|\}$, as functions of the normalized frequency (ω). In these computations $k = (\omega)\sin(\theta)$.

3. The presence of resonances

The standard computations are presented in Fig. 2. These computations are carried out with the standard parametric values: $(\eta) = (10^{-2})$, $(\eta_c) = (10^{-2})$, $(\eta_m) = (10^{-2})$, $(\eta_p = (10^{-2})$, $(\omega_c) = (10)$, $(k) = (0)$, $(b_1) = (0)$ and $(b) = (\pi)$, in place. Also when the standard baffle is present, the modulus of the reflection coefficient $|R(\omega)|$ is largely equal to unity, implying, thereby, that the absorption in the surface of the baffle is negligible. On the other hand, the standard removal of the baffle is accomplished by rendering the modulus of the reflection coefficient $|R(\omega)|$ negligible, implying, thereby, that the absorption in the surface of the baffle is total. Imposing these standard values Fig. 2 is obtained. Fig. 2 exhibits the following quantities:

Fig. 2a depicts $|T_{bc}(o,\omega)|$ in the solid curve and $|T_c(o,\omega)|$ in the dotted curve, Fig. 2b depicts $|T_b(o,\omega)|$ in the solid curve and $|T(0,\omega)|$ in the dotted curve, Fig. 2c depicts $|T_{bc}(o,\omega)/T_b(o,\omega)|$ in the solid curve and $|T_c(o,\omega)/T(o,\omega)|$ in the dotted curve.

The footprints of the cavity are clearly demonstrated in both, Fig. 2a in the presence of the coating and Fig. 2b in the absence of the coating. The influence of the coating is accentuated in Fig. 2c where the ratio of the transfer functions in the presence of the coating to those in the absence of the coating are depicted;i.e., the curves in Fig. 2a are divided by those in Fig. 2b to obtain Fig. 2c. Evidently, the resonances and the anti-resonances that the cavity generates dominate the scenes in Fig. 2. Also clearly, the resonances and anti-resonances are absent in the absence of the baffle and, therefore, in the absence of the cavity. [The absence of the cavity may be

achieved by rendering (b) infinite;i.e., the baffle is removed onto a plane an infinite normalized distance below the plate. One recalls that in this paper distances are normalized by (c_1/ω_o). The transition from a finite normalized spatial extent, in which resonances and anti-resonances are generated, to the semi-infinite normalized spatial extent in which resonances and anti-resonances are absent is thus demonstrated [8].] Figs. 3–5 repeat Fig. 2 except that the loss factor (η) in the cavity is increased from the standard value of (10^{-2}) in Fig. 2 to (10^{-1}) in Fig. 3 and to (3×10^{-1}) in Fig. 4 and, finally, to (5×10^{-1}) in Fig. 5. Figs. 3–5 show that the resonances and the anti-resonances are suppressed more and more by these successive increases in damping.However, the phenomenon of suppressed resonances and anti-resonances is not missing in Fig. 2. The suppression in Fig. 2 occurs merely at a higher frequency range than in Fig. 3. To explain this phenomenon one recalls that the degree of damping is not sufficiently stated by merely specifying the loss factor [2,9,10]. One must also specify the normalized frequency separation ($\Delta\omega$) between adjacent resonances. A modal overlap parameter (B) may then be defined formally as

$$B(\omega) = (\omega\eta_e/\Delta\omega) = (\omega\eta_e)\mathrm{n}, \quad \Delta\omega = [\mathrm{n}]^{-1}, \quad \mathrm{n} = \mathrm{n}(\omega), \quad \eta_e = \eta_e(\omega), \tag{17a}$$

where n(ω) is the local (normalized) *modal density* and $\eta_e(\omega)$ is the corresponding local *effective loss factor* in the dynamic system. [It is recalled that ($\omega\eta_e$) is the normalized frequency bandwidth

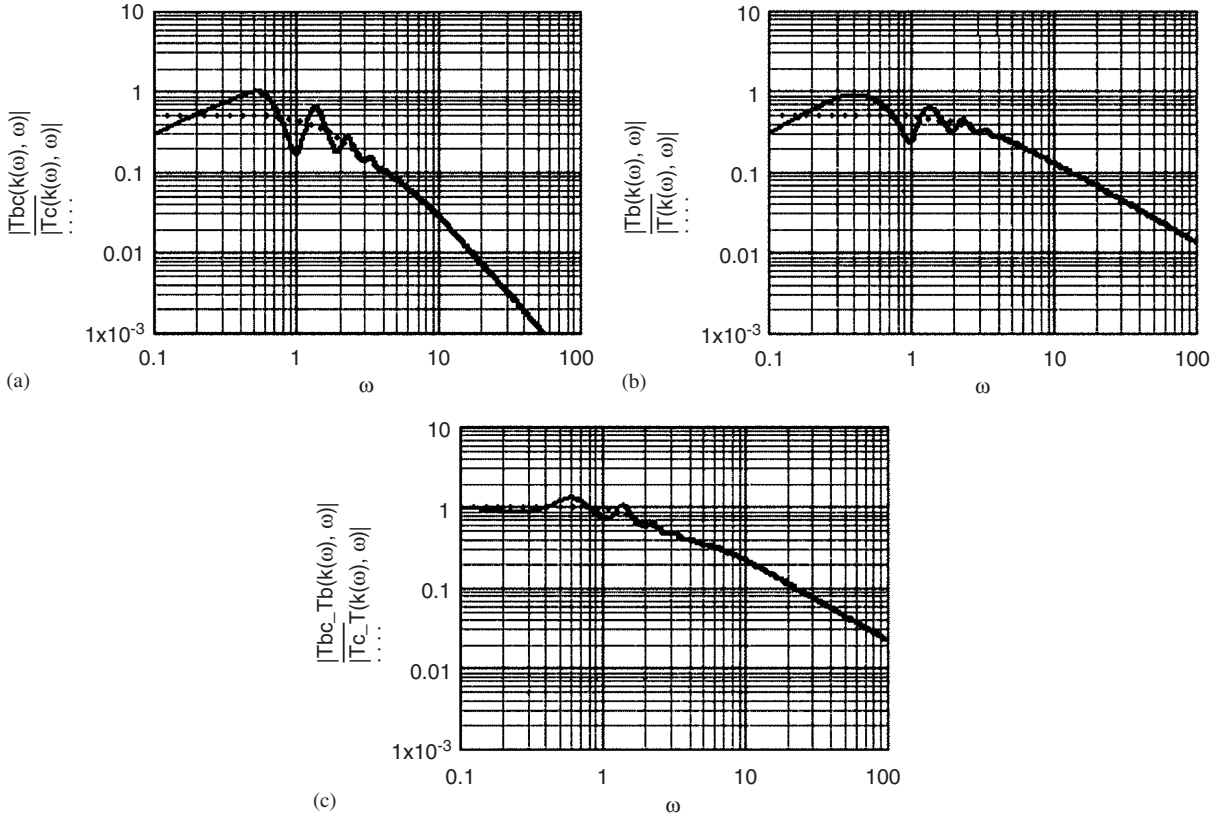

Fig. 3. The same as Fig. 2 except that (η) is changed from the standard value of (10^{-2})–(10^{-1}).

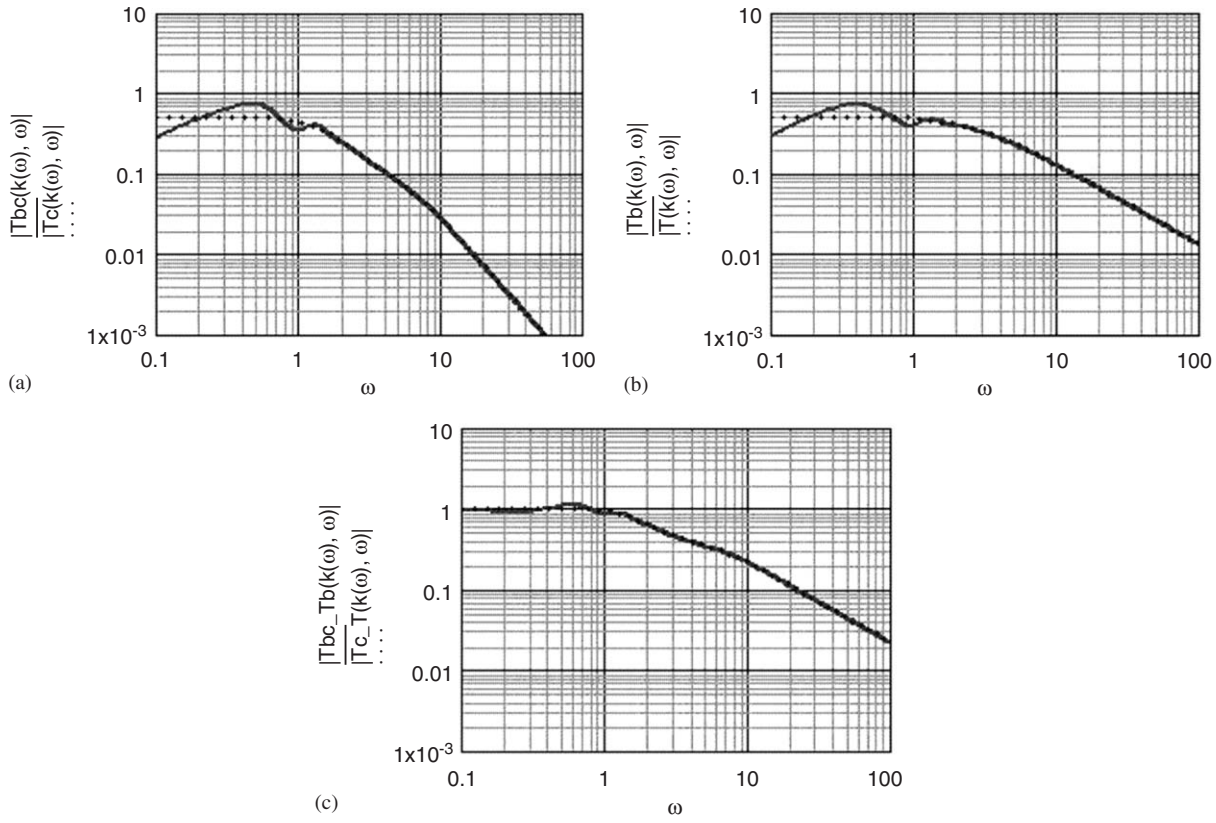

Fig. 4. The same as Fig. 2 except that (η) is changed from the standard value of (10^{-2})–(3×10^{-1}).

of a local resonance or a local anti-resonance.] The degree of damping is then defined in terms of (B) in the form

$$B = \begin{cases} \ll 1 & \text{light damping,} \\ \cong 1 & \text{mid-damping,} \\ \gg 1 & \text{high damping.} \end{cases} \tag{18a,b,c}$$

In the frequency locality where the local (B) is less than unity, resonances and anti-resonances dominate the scene. In the frequency locality where the local (B) approaches unity, resonances and anti-resonances approach indistinguishability. Finally, in the frequency locality where the local (B) exceeds unity, resonances and anti-resonances are suppressed. In Fig. 2 in the presence of the cavity the modulus of the reflection coefficient $|R(\omega)|$ is conditioned to be substantially equal to unity throughout the normalized frequency range of interest here; namely, $0.1 < \omega < 10^2$. Thus, in this figure, the modal overlap parameter $B(\omega)$ is dominated by the volume (bulk) loss factor (η). This $B(\omega)$ is given by

$$B(\omega) \Rightarrow B_o(\omega) = (\omega\eta)\mathrm{n}, \quad k = \omega \sin(\theta) = 0 \tag{17b}$$

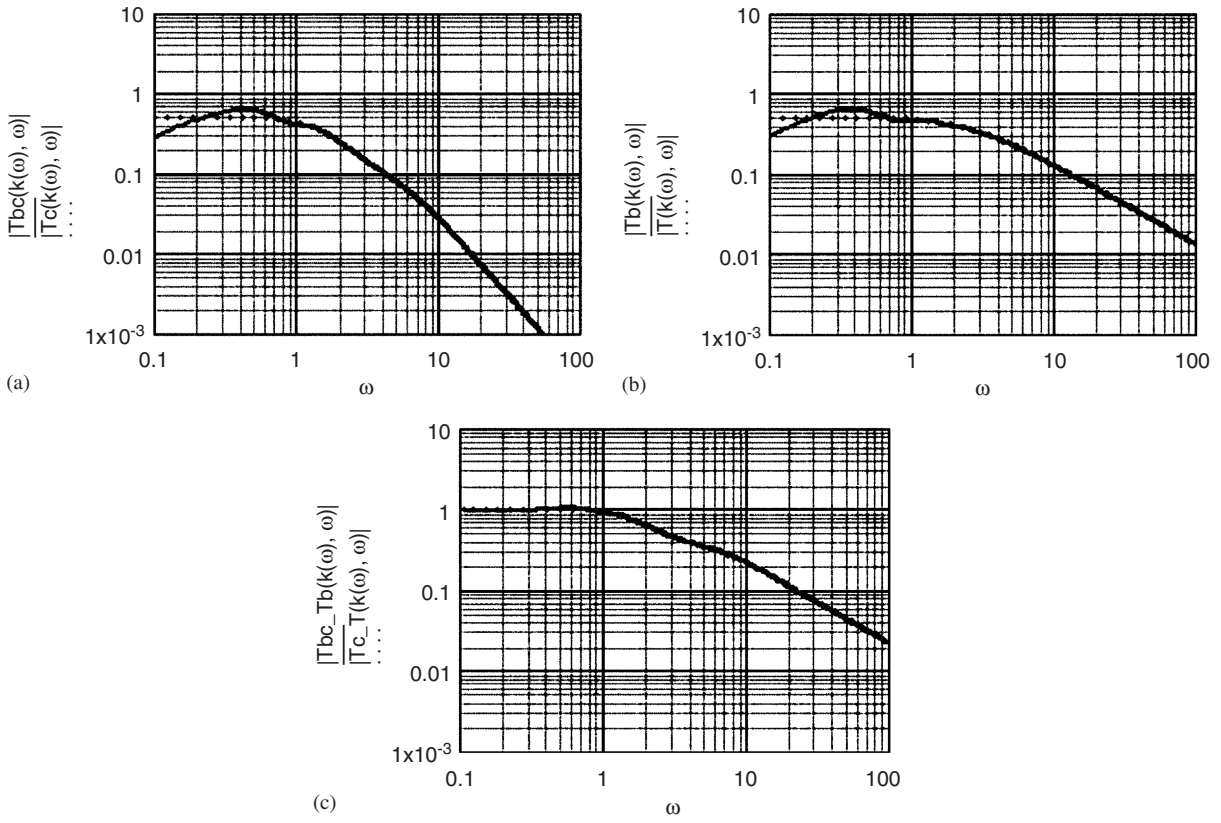

Fig. 5. The same as Fig. 2 except that (η) is changed from the standard value of (10^{-2})–(5×10^{-1}).

[cf. Appendices A and B]. In Fig. 2, both the loss factor (η) and the normalized modal density (n) are assumed to be independent of (ω) so that the modal overlap parameter $B_o(\omega)$ is simply proportional to (ω). This simple proportionality explains the gradual suppression of the resonances and the anti-resonances as the normalized frequency (ω) increases. In fact, as the normalized frequency increases to render (B_o) in excess of unity, the suppression is complete. This phenomenon is, exhibited in Fig. 2. The successive increases in (η), depicted in Figs. 3–5, introduce suppressions of the resonances and the anti-resonances similar to those exhibited in Fig. 2. However, compared with Fig. 2, the suppressions in Figs. 3–5 suffer proportional shifts to lower and lower frequencies along the normalized frequency axis as (η) increases successively. The suppressions are shifted successively to the lower and lower normalized frequency range. [In Appendix A it is shown that n = 1 in Figs. 2–5 and, therefore, the modal overlap parameters in these figures are, governed merely by $B_o(\omega) = (\omega\eta)$.] A rough estimate in Figs. 2–5 would convince one that Eqs. (17) and (18) in the text and Eqs. (A.1)–(A.8) in Appendix A appear to be validated. In addition to confirming these equations, it appears in Figs. 2–5 that in those regions of the normalized frequency domain where the local modal overlap parameter (B_o) exceeds unity, the solid curve locally coalesces with the dotted curve. It is recalled that the solid curve pertains to the presence of the cavity and the dotted curve pertains to the absence of the cavity. This local

coalescence of the two curves, exemplifies "The mean-value method of predicting the dynamic response of complex vibrations" proposed by Skudrzyk [11].

It has been established that there exists a reasonable correspondence between the absorption on the surface of the baffle and the volume (bulk) absorption represented by the loss factor (η). In this vein, it may be useful to cast the modulus of the reflection coefficient $|R(\omega)|$ in the form

$$|R(\omega)| \Rightarrow |R| = \exp[-(r_b)], \tag{19a}$$

where (r_b) is positive, is real and is assumed to be independent of (ω). Thus, in Figs. 2–5 the value of (r_b) is conditioned to be equal to (10^{-3}), rendering $|R|$ substantially equal to unity. The value of $r_b = (10^{-3})$ is the designated standard. The standard value of (r_b) is changed in a manner reminiscent of the changes in (η) depicted in Figs. 3–5. The changes in (r_b) are from the standard value of (10^{-3}) to $(2\pi \times 10^{-1})$ to (2) and, finally, to (π). The influence of these changes is depicted in Figs. 6–8, respectively, with Fig. 2 serving, again, as the standard base. In Figs. 6–8 the volume loss factor (η) is maintained at the standard value of (10^{-2}). Therefore, only at the higher normalized frequency range, where $\omega > 50$, does the value of (B_o) approach unity. As explained in Appendix A the contribution of $B_b(\omega)$ to the modal overlap parameter $B(\omega)$ by the absorption at the surface of the baffle is given by

$$B(\omega) = B_b(\omega) + B_o(\omega), \quad B_b(\omega) = (r_b/2\pi), \quad k = \omega \sin(\theta) = 0. \tag{17c}$$

The increases in (r_b) that are depicted in Figs. 6–8 are compared with the corresponding increases in (η) in Figs. 3–5, respectively. Figs. 6–8 and 3–5 show similar departures from Fig. 2. Moreover, the features in Figs. 6–8 can be similarly interpreted in the light of Figs. 3–5 vis à vis Fig. 2. Indeed, the absorption in the surface of the baffle are quite similar to the absorption in the body of the fluid (fluid no. 2) in the cavity, not a surprising similarity to a noise control engineer. The difference lies in that the influence of the loss factor in the function $[\exp\{a(k,\omega)\}]$ is made frequency dependent, whereas the reflection coefficient, as assumed here, is not. In particular, from Eq. (7), and with the assistance of Appendix A, one finds

$$|\exp\{a(k,\omega)\}| = \exp[-2(\omega\eta)(c_1/c_2)(b)k_2(k,\omega)],$$

$$k = \omega \sin(\theta), \quad 0 \leqslant \theta < (\pi/2), \tag{19b}$$

where (η) is assumed to be largely frequency independent and (b) is the normalized separation between the plate and the baffle; i.e., (b) is the normalized width of the cavity. Comparisons between Figs. 6–8 and 3,4,5, respectively, reveal that differences in details exist. Although the differences may be adequately interpreted by the material presented in Appendix A, dealing with these differences, in addition to the above discussion, is, however, beyond the scope of this paper.

4. Suppressing the resonances (and anti-resonances) by replacing summations by integrations

One learnt that the damping, including that contributed by the absorption in the surface of the baffle, tends to converge the solid curves onto the dotted curves in Figs. 2–8. The convergence is particularly complete in those ranges of the frequency for which the local modal overlap parameters exceed unity. It is proposed that the action of converting summations over modes to

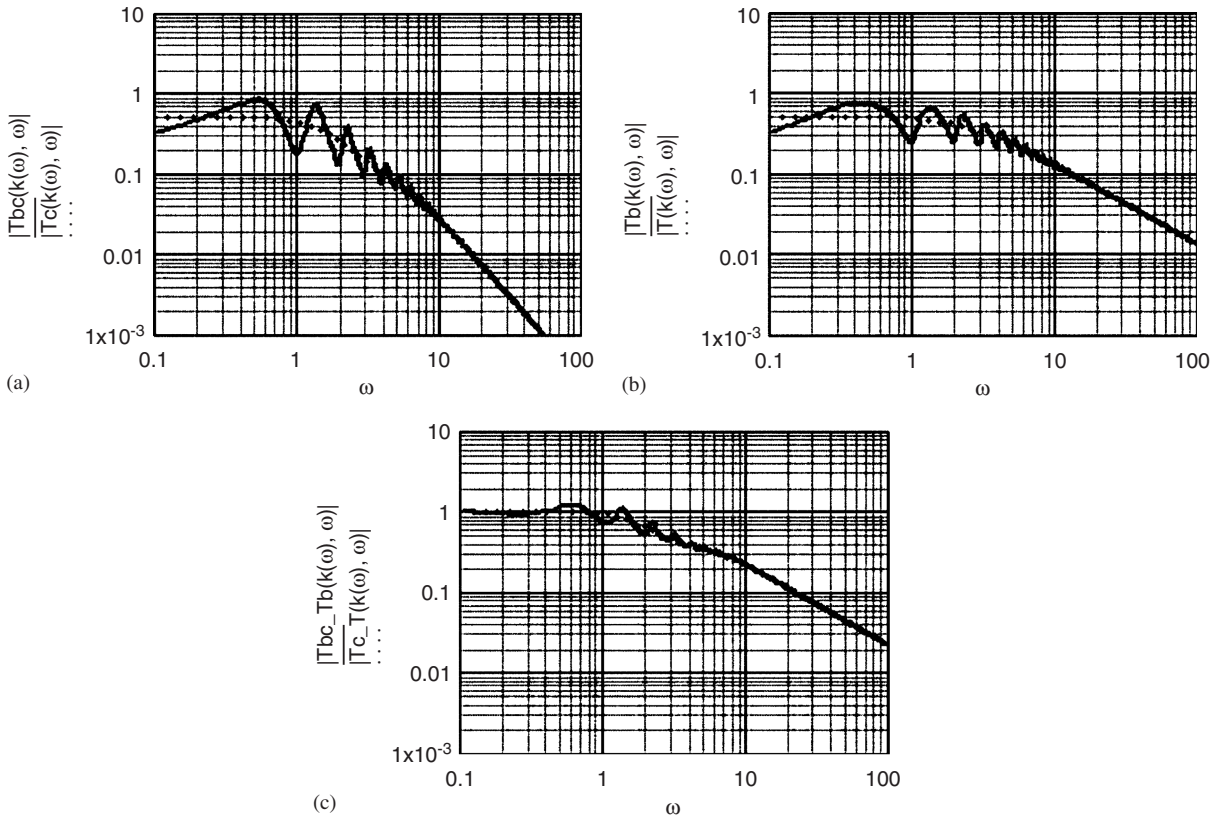

Fig. 6. The same as Fig. 2 except that $|R(\omega)|$ is changed from the standard value of $[\exp(-10^{-3})]$–$[\exp(-2\pi \times 10^{-1})]$.

integrations is equivalent to increasing the value of the modal overlap parameters in those locations in the frequency domain in which the inherent value of the modal overlap parameters lie below unity. By contrast, in those regions in the frequency domain in which the value of the local modal overlap parameters exceed unity, converting summations to integrations is appropriate. In these regions the integrations are *commensurate* with the summations over a *continuous* distribution of modes [1,5]. The continuity, it is emphasized, is conditioned by the value of the local modal overlap parameters that exceed unity; neither the value of the local (normalized) modal densities alone nor the value of the local loss factors alone will suffice to ensure adequately this continuity [2]. One may wonder how this should be interpreted. From Figs. 2–8 as just stated, the absorption in the cavity tends to bring the solid curves to converge onto the dotted curves. This convergence is completed when the absorption is high enough to be commensurate with the removal of the cavity. This removal may be in the form of increasing (b) to infinity which amounts to gradually rendering the bottom fluid (fluid no. 2) semi-infinite. Recall that the top fluid (fluid no. 1) is ab initio semi-infinite. When the increase is final, the solid curves are then coincident with the dotted curves [8]. It is also observed in Figs. 2–8 that the excursions in the solid curves, manifesting the resonances and the anti-resonances, diminish as the value of the local modal

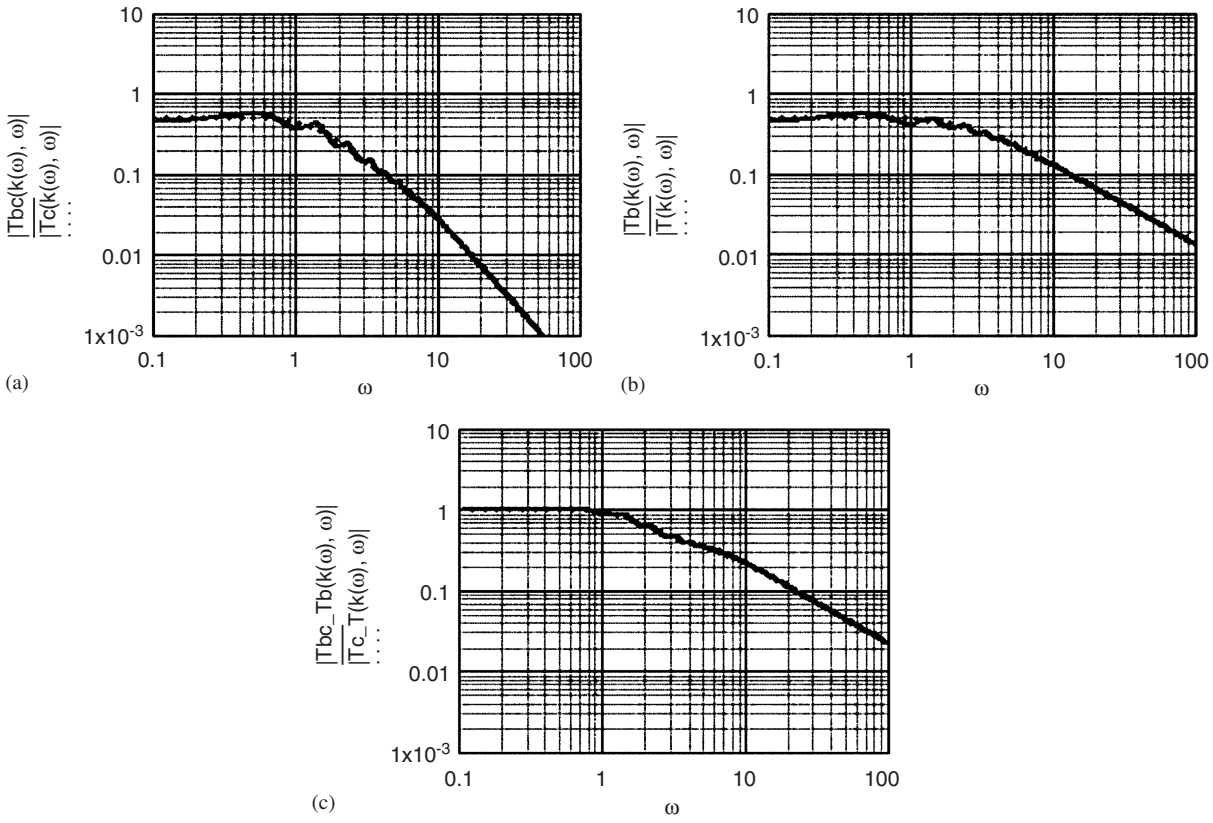

Fig. 7. The same as Fig. 2 except that $|R(\omega)|$ is changed from the standard value of $[\exp(-10^{-3})]$–$[\exp(-2)]$.

overlap parameter $B(\omega)$ increases toward unity and beyond, notwithstanding that the dotted curves remain unchanged by these increases in $B(\omega)$. Indeed, it is observed in these figures that the dotted curves serve as the geometrical mean to the positive excursions of the resonances with the negative excursions of the adjacent anti-resonances. [It is to be recalled that resonances and anti-resonances form adjacent pairs.] This geometrical mean then remains unchanged by (reasonable) changes in the value of the local modal overlap parameter $B(\omega)$ [12,13]. Thus, as far as this geometrical mean is concerned, resonances and anti-resonances may be artificially added andmodified to close the gaps between adjacent peaks and nadirs even in those frequency regions where $B(\omega)$ is less than unity. These insertions and modifications, which result in higher modal densities and/or in higher loss factors, may effectively render $B(\omega)$ in excess of unity in any desired region in the frequency domain. This rendering a priori causes the solid curves to be coincident with the dotted curves, thereby, indicating that in this region the resonances and that the anti-resonances are indistinguishable and the transition along the normalized frequency axis is smooth. It is this contrived smoothness that allows one to convert the thorny summations into integrations. After all, the allowed artificial insertions and modifications of resonances and anti-resonances render the modal distribution continuous. Conversely, when summations are

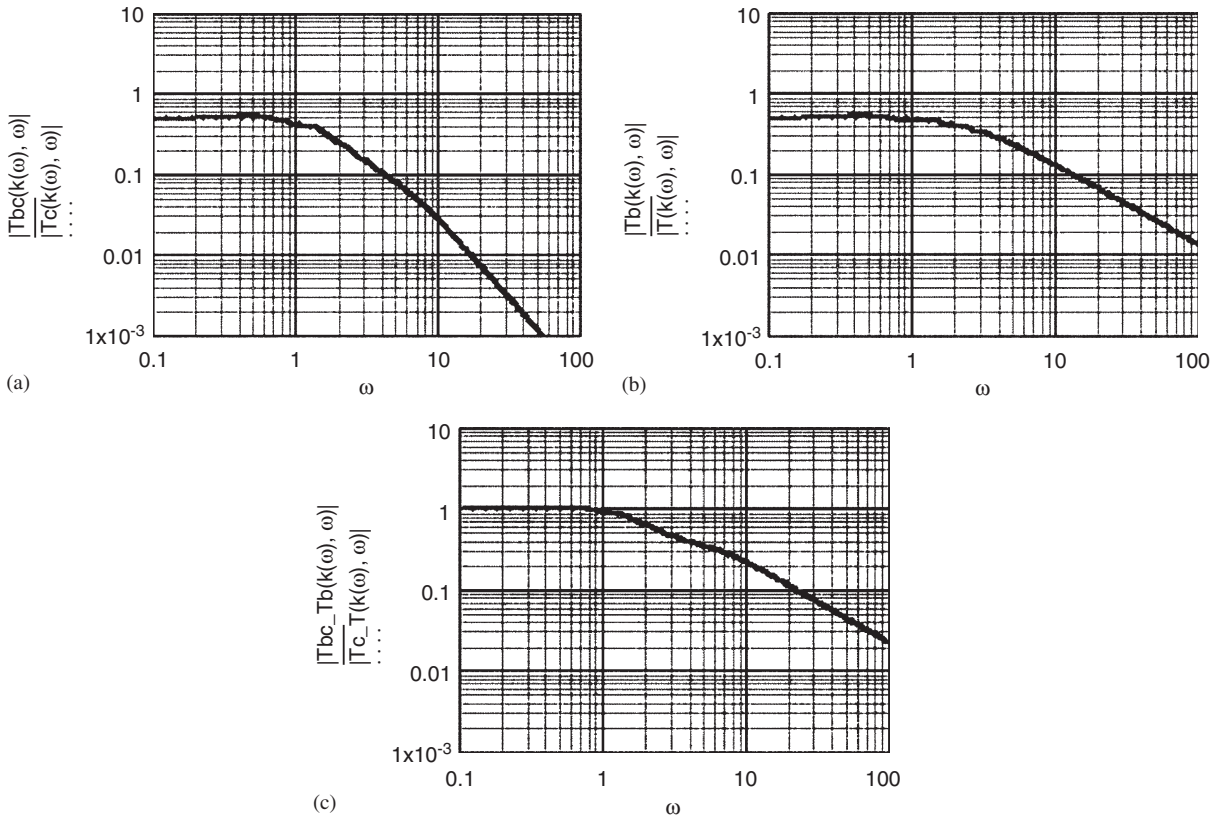

Fig. 8. The same as Fig. 2 except that $|R(\omega)|$ is changed from the standard value of $[\exp(-10^{-3})]$–$[\exp(-\pi)]$.

converted to integrations, this artificial insertion and modification of resonances and anti-resonances is implied a priori. Can this contention be illustrated by analysis and by computations? To illustrate, one needs to revisit Eq. (7). The resonances and the anti-resonances are generated in this equation by the factors that represent summations. These factors and their representation by summations are

$$[1 + R(\omega)\exp\{\mathrm{a}(k,\omega)\}]^{-1} = \sum_{m=0}^{\infty} [-R(\omega)\exp\{\mathrm{a}(k,\omega)\}]^m, \tag{20a}$$

$$[1 - R(\omega)\exp\{\mathrm{a}(k,\omega)\}]^{-1} = \sum_{m=0}^{\infty} [R(\omega)\exp\{\mathrm{a}(k,\omega)\}]^m \tag{20b}$$

$$[1 + (-1)^s R(\omega)\exp\{\mathrm{a}_1(k,\omega)\}]^{-1} = \sum_{m=0}^{\infty} [(-1)^{s+1} R(\omega)\exp\{\mathrm{a}_1(k,\omega)\}]^m, \tag{20c}$$

where one is reminded that (s) is an index designating the pole nature of the external drives; e.g., $s=0$ designates monopole-like and $s=1$ designates dipole-like external drives. The conversion of these summations to integrations yields

$$[1+R(\omega)\exp\{\mathrm{a}(k,\omega)\}]\Rightarrow 1, \tag{21a}$$

$$[1-R(\omega)\exp\{\mathrm{a}(k,\omega)\}]\Rightarrow 1, \tag{21b}$$

$$[1+(-1)^{s}R(\omega)\exp\{\mathrm{as}(k,\omega)\}]\Rightarrow 1, \tag{21c}$$

respectively, where use is made of the identity

$$\ln[X(k,\omega)]\int_0^{\infty}[X(k,\omega)]^{y}\,\mathrm{d}y=1. \tag{22}$$

Substituting Eq. (21) in Eq. (7) renders $A(k,\omega)$ and $C(k,\omega)$ equal to unity. This substitution then renders

$$T_{bc}(k,\omega)\Rightarrow T_{c}(k,\omega),\quad T_{b}(k,\omega)\Rightarrow T(k,\omega), \tag{23}$$

respectively. Eq. (23) may be verified employing Eqs. (11) and (12) and Eqs. (10) and (15), respectively. As contended, the conversion of the summations to the corresponding integrations, indeed, suppresses the resonances and anti-resonances in the transfer functions of concern. Again, examining Eq. (21) reveals that this suppression is commensurate with assigning a total absorption at the baffle, which renders $|R(\omega)|\Rightarrow 0$. This condition, in turn, is commensurate with the removal of the cavity. The conditions that are obeyed in Fig. 2 are augmented by Eq. (21) and the moduli of the transfer functions $|T_{bc}(k,\omega)|$, $|T_{b}(k,\omega)|$, $|T_{c}(k,\omega)|$ and $|T(k,\omega)|$, are computed. The results of these computations are depicted in Fig. 9. The solid curves in Fig. 9 are those in Fig. 2 except that the summations are converted to the corresponding integrations as prescribed in Eqs. (20) and (21). A comparison of Fig. 9 with Fig. 2 would rest the contention made in this section, if not in the paper as a whole. Nonetheless for the record, it may be useful to restate the contention in bolder terms. Eqs. (1), (7), (20) and (21), in unison, declare that the transfer functions, when summations are converted to corresponding integrations, become *independent* of the *effective* loss factor (η_e). This loss factor describes the sum of both volume and surface absorptions in the cavity; $\eta_e=(\eta_b+\eta)$. This *independence*, it is argued, allows one to assume that (η_e) may be set as small as one wishes, without changing the transfer functions [1–6]. Setting (η_e) small, without invoking a proper criterion to computing Fig. 9, may be misleading, as Fig. 10 attests. Fig. 10 repeats Fig. 2 except that, whereas (r_b) remains equal to (10^{-3}), (η) is changed from the standard value (10^{-2}) in Fig. 2 to (10^{-4}) in Fig. 10. The ratio of the effective loss factor $(\eta_e)_{10}$ in Fig. 10 to the effective loss factor $(\eta_e)_2$ in Fig. 2 is then

$$[(\eta_e)_{10}/(\eta_e)_2]=[(5/\pi)+\omega][(5/\pi)+10^{2}\omega]^{-1}\ll 1,\quad 0.1<\omega<10^{2}. \tag{17d}$$

Under the criterion for converting the summations to integrations, Fig. 9 is common to Figs. 10 and 2 [7]. Yet, Fig. 9 does not only hide the presence of resonances and anti-resonances in Fig. 2, but it hides the differences between Figs. 2 and 10. These differences are accounted for by Eq. (17d). What would Fig. 9 hide were one tempted to render the effective loss factor (η_e) vanishingly small [9,10]?

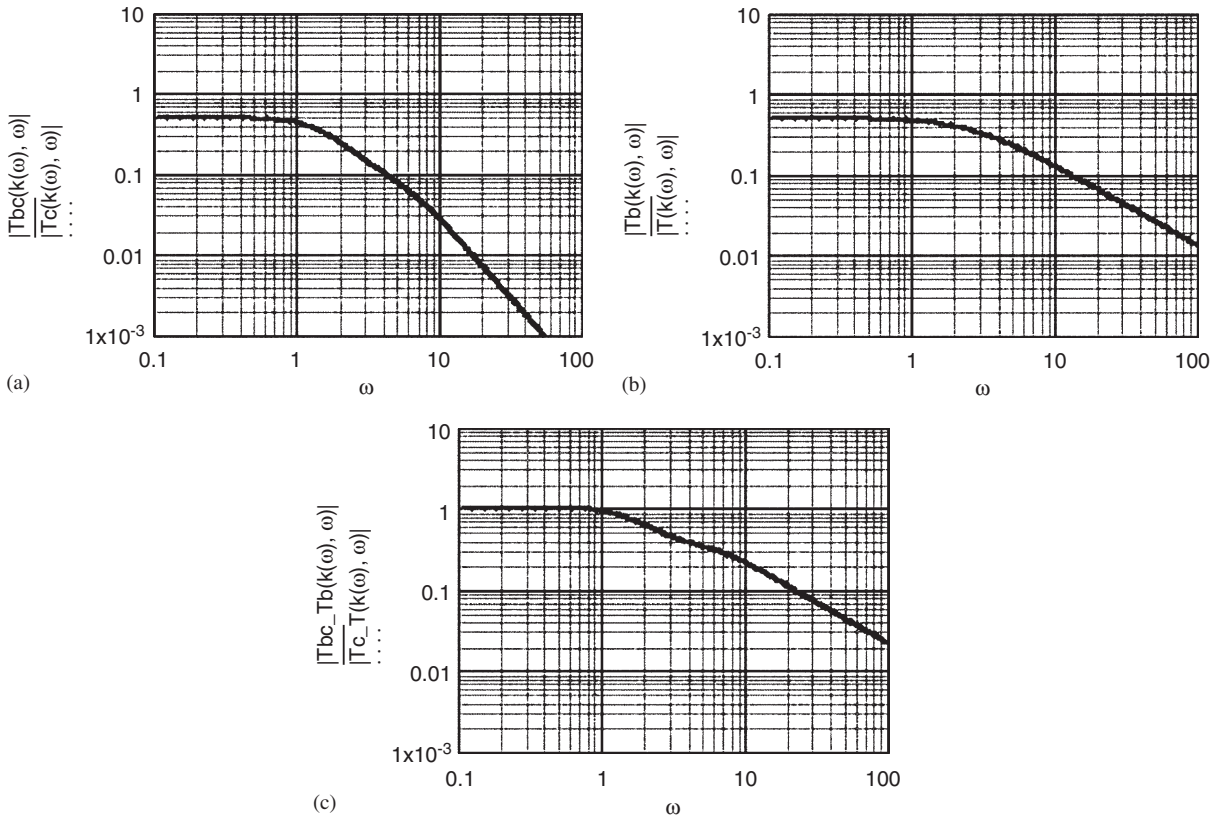

Fig. 9. The same as Fig. 2 except that the conditions are augmented by those stated in Eq. (21). These augmented conditions are tantamount to rendering $|R(\omega)|$ substantially equal to zero; $|R(\omega)| \Rightarrow 0$.

Finally, both the resonances and anti-resonances are prominently present in the foregoing considerations. In most practical situations, even when the resonances are clearly distinguishable, the anti-resonances are usually obscured by noise. Thus, the peaks in the resonances may be visible and identified, but the nadirs in the anti-resonances are hidden within the noise. The geometrical averaging is, therefore, not readily implemented. The averaging that is usually implemented under these circumstances tends to rise above the geometrical average. As is argued, a noise control measure; e.g., increase in damping, will tend to bring the response, as expressed for example by the transfer function considered here, toward the geometrical mean *à la* Skudrzyk [11]. In practice, the increase in damping also will cause an increase in the levels of the nadirs of the anti-resonances. This *detriment*, however, is obscured by the noise (What the eye does not see, the heart does not grieve!). The merit of the damping, in the initial stages of increasing it may thereby be exaggerated. *Nonetheless*, *once the geometrical mean-level has been reached*, *further increases in damping*, *that will render the modal overlap parameter to exceed unity*, *would be of no practical benefit*. The resonances and the anti-resonances can hardly reverse their roles and a beneficial saturation will prevail.

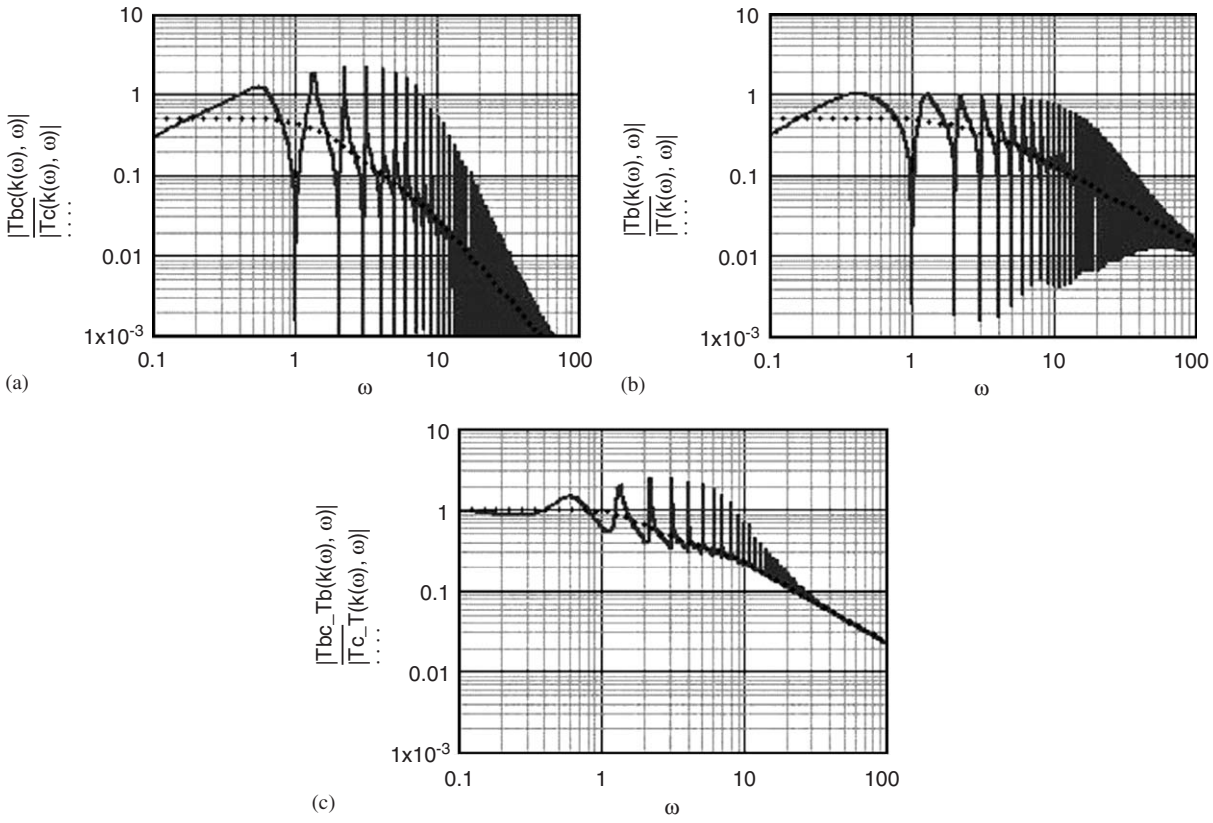

Fig. 10. The same as Fig. 2 except that (η) is changed from the standard value of (10^{-2})–(10^{-4}).

Acknowledgements

The work described in this paper was supported by ONR and In-House funding.

Appendix A

The contributions to the modal overlap parameter by the absorption in the surface of the baffle and in the volume of the cavity.

In order to carry out a number of computations it becomes necessary to state more explicitly the parameters that define the dynamic system. Of particular significance are the analytical forms for the normalized modal densities and the loss factors. Through these parameters, the analytical expressions for the modal overlap parameters may then be derived. In this vein, the normalized modal density n(ω) of the resonances (and of the anti-resonances) in the dynamic system here considered may be simply ascertained. [The modal density is the inverse of the frequency separation ($\Delta\omega$) between adjacent resonances. The *normalized* modal density pertains to the

normalized frequency separation.] For this purpose the reflection coefficient (R) is cast in the form

$$R(\omega) = \exp[-r_b(\omega) - ir_I(\omega)] \tag{A.1}$$

with (r_b) and (r_I) real parameters. Recalling Eq. (7) the local (normalized) modal density n(ω) assumes, by definition, the expression

$$[2\pi \mathrm{n}(\omega) - \{\partial r_I(\omega)/\partial\omega\}] = A_b, \quad k = k(\omega) < \omega,$$

$$A_b = 2(c_1/c_2)(b)[k_2(k,\omega)], \tag{A.2}$$

where it is assumed that the normalized width (b) of the cavity is independent of the normalized frequency (ω) and the normalized wavenumber (k) is restricted to the supersonic range; in this case $k_2(k,\omega) \Rightarrow k_2[\omega \sin\theta, \omega]$. Again the angle ($\theta$) is the direction, off the normal to the plane of the plate, of radiation into the top fluid (fluid no. 1) by the emerging supersonic component on the interface with that top fluid. Similarly, an *equivalent volume* (or bulk) loss factor may be defined to account for the absorption in the surface of the baffle. This local loss factor is designated (η_b) and the expression for it is

$$(\omega\eta_b) = [r_b(\omega)/A_b], \quad k = k(\omega) < \omega. \tag{A.3}$$

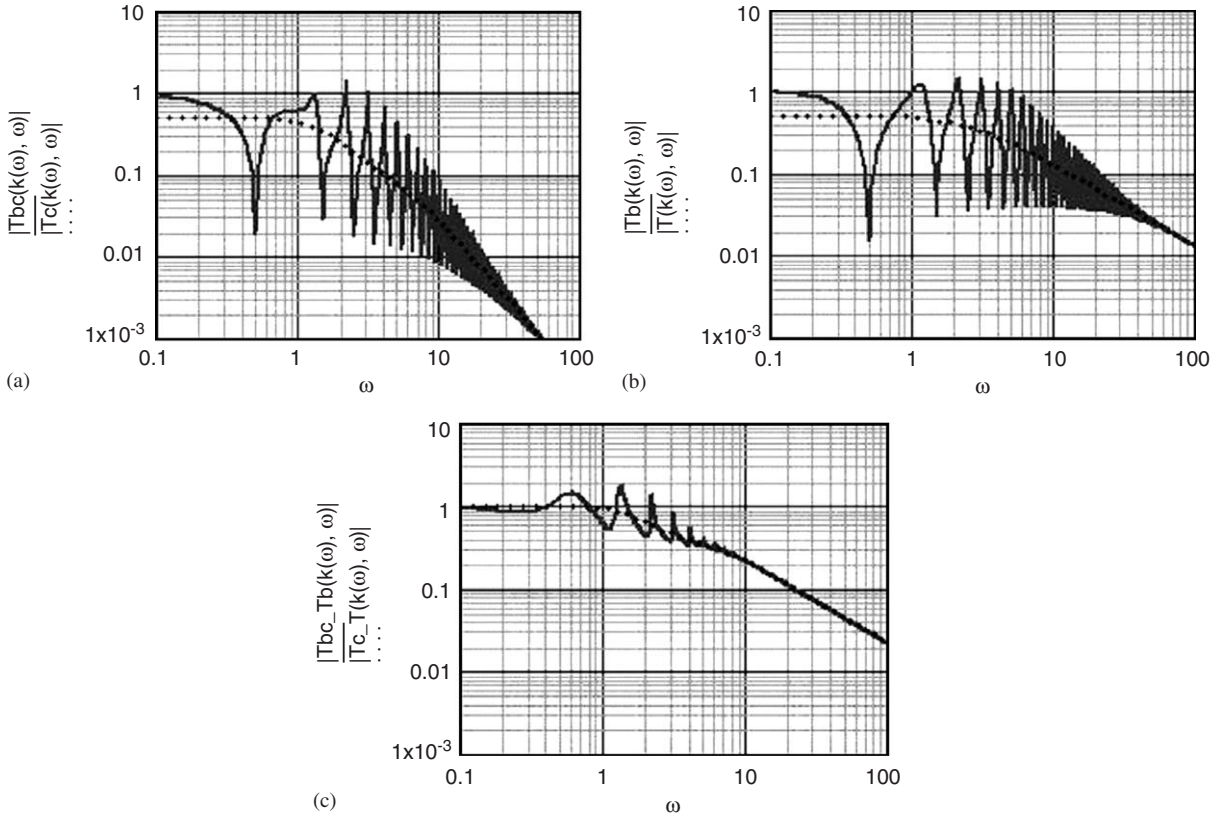

Fig. B1. The same as Fig. 2 except that the standard dipole-like external drive with $s = 1$, is changed to monopole-like with $s = 0$.

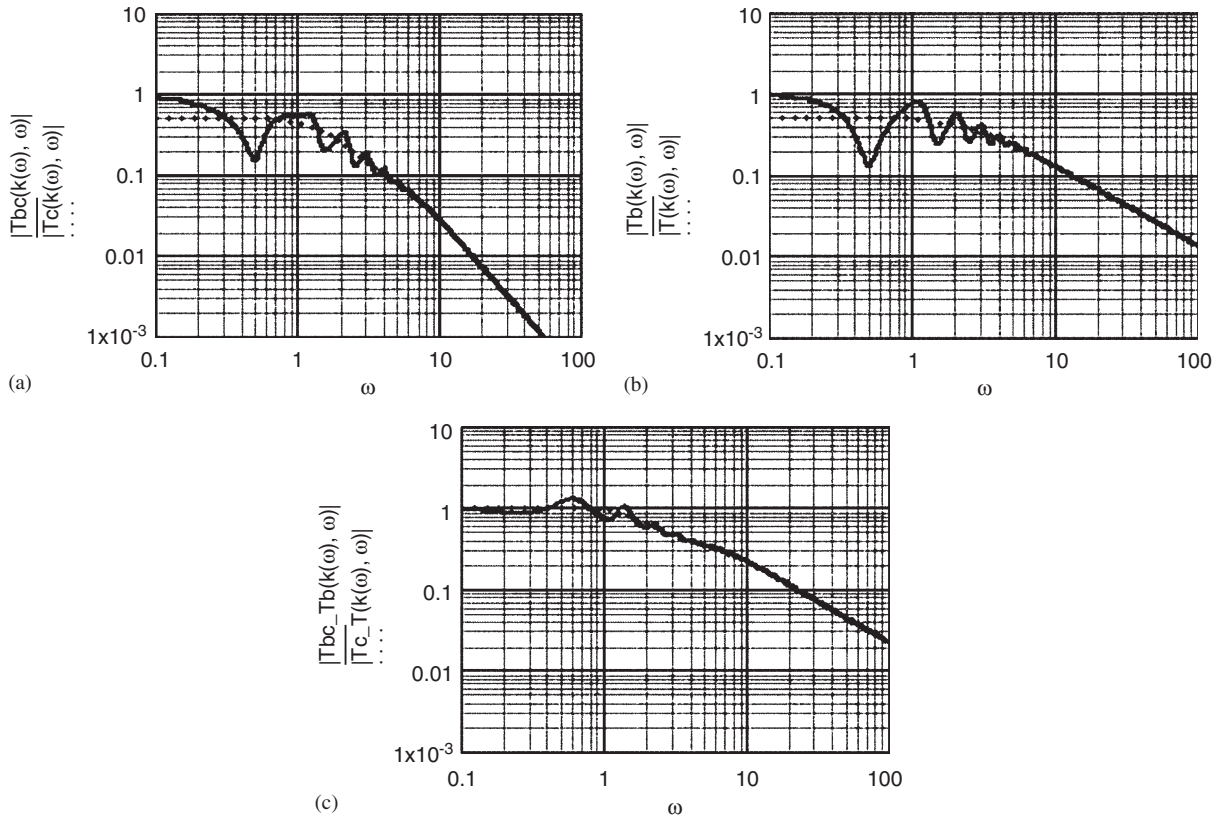

Fig. B2. The same as Fig. 3 except that the standard dipole-like external drive with $s = 1$, is changed to monopole-like with $s = 0$ [cf. Fig. 2].

In this connection, (η) is the volume (or bulk) loss factor in the cavity. The local modal overlap parameter $B(\omega)$, in the cavity here considered, may then be determined in the two-components form

$$B = B_b + B_o, \quad B_b = (\omega\eta_b)\mathrm{n}(\omega), \quad B_o = (\omega\eta)\mathrm{n}(\omega) \tag{A.4}$$

[cf. Eq. (17)]. Substituting Eqs. (A.2)–(A.4) in the factor $[R(\omega)\exp\{\mathrm{a}(k,\omega)\}]$ in Eq. (7), one may show that the absolute value of this factor may be cast in the form

$$|R(\omega)\ \exp\{\mathrm{a}(k,\omega)\}| = \exp[-\{\omega\eta_e(\omega)\}A_b],$$

$$\eta_e(\omega) = \eta_b(\omega) + \eta(\omega), \tag{A.5}$$

where $\eta_e(\omega)$ is the effective loss factor in the cavity [cf. Eq. (17a)]. Merely for the sake of simplicity and convenience (r_I), (r_b) and (η) are assumed to be independent of (ω). It is further decreed that the computations are to be carried out for components for which

$$k = \omega\sin(\theta), \quad k_2(k,\omega) = k_2[\omega\sin(\theta),\omega] \tag{A.6a}$$

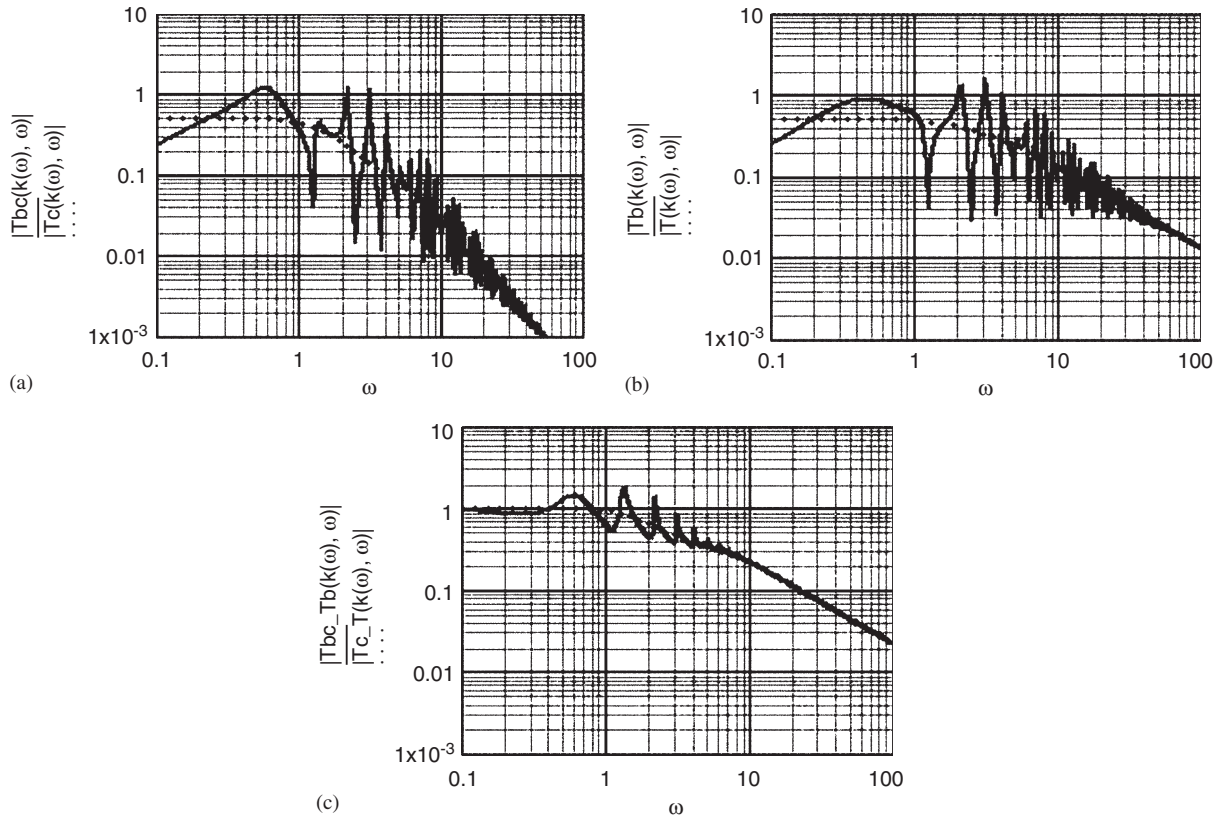

Fig. B3. The same as Fig. 2 except that the value of (b_1) is changed from the standard value of zero to $(b_1) = 0.2$ (b). Again, note that (b) and (b_1) are normalized quantities.

and if $c_1 = c_2$ then

$$k_2(k, \omega) = k_2 = \cos(\theta), \tag{A.6b}$$

and, therefore, (k_2) is independent of the normalized frequency (ω) and the angle (θ) is the directional designation of a (supersonic) component on the interface with the top fluid (fluid no. 1). Imposing Eqs. (A.6b) on Eq. (A.5) reduces this equation to read

$$|R(k, \omega)\exp\{\mathrm{a}(k, \omega)\}| \Rightarrow \exp[-\{r_b + (\omega\eta)A_b\}],$$

$$A_b \Rightarrow 2[(b)\cos(\theta)] \tag{A.7}$$

and then one finds that

$$(\omega\eta_b) = (r_b/2)[b\ \cos(\theta)]^{-1}, \quad \mathrm{n} = (\pi)^{-1}[b\cos(\theta)],$$

$$B_b = (r_b/2\pi), \quad B_o = (\omega\eta)(\pi)^{-1}[b\cos(\theta)]. \tag{A.8}$$

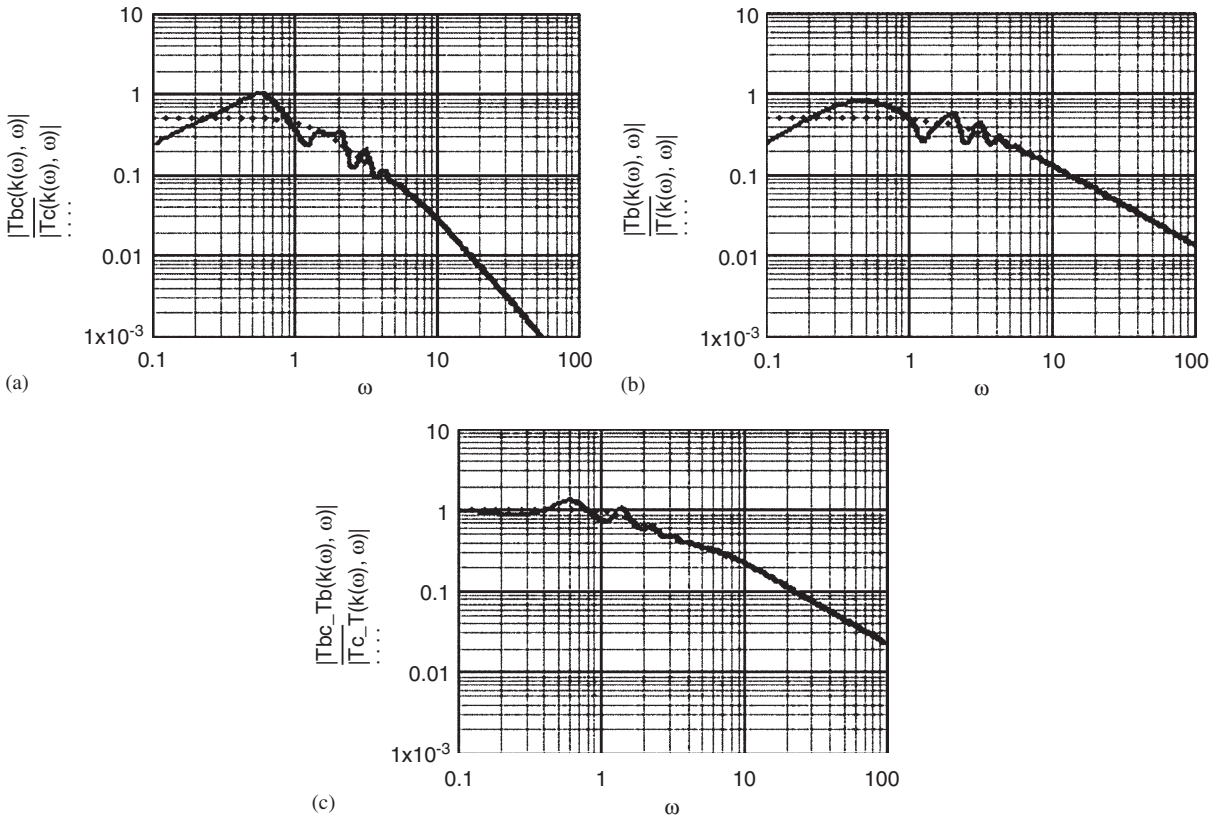

Fig. B4. The same as Fig. 3 except that the value of (b_1) is changed from the standard value of zero to $(b_1) = 0.2(b)$ [cf. B3].

Appendix B

Variations in the propagation and the separation distance in the cavity as well as in the nature of the external drive.

A number of computational variations on the theme depicted in the text are exemplified. The purpose of this appendix is to show the versatility of the computational breadth of the analysis. However, this analysis is used here exclusively toward the arguments that lie within the scope chosen for this paper. The analysis and the model employed could, in the future, serve a wider and a more extended scope. In this vein, in Fig. B1, Fig. 2 is repeated except that the external drives are changed from the standard dipole-like with $s = 1$, to a monopole-like, with $s = 0$ [cf. Eq. (7b)]. The influence of this change can be observed in comparing Fig. 2 with Fig. B1. There is a difference not only in the dispositions of the resonances and anti-resonances but also in their excursions at the higher frequency ranges. Indeed, they converge more slowly on to the geometrical mean with an increase in frequency than when $s = 0$. However, the difference is insignificant to the arguments conducted in this paper. To emphasize this point Fig. B2 is shown. In this figure, Fig. 3 is repeated with $s = 0$. The relationship between Figs. B1 and B2 are similar to those between Figs. 2 and 3. On the same theme Fig. B3 is offered. The external drives which

are placed in Fig. 2 on the standard plane at (b_1) equal to zero, are now placed at $(b_1) = 0.2b$. Again, there is a difference between Figs. 2 and B3 that is similar, in certain aspects, to the difference between Figs. 2 and B1. This difference is also insignificant to the arguments conducted in this paper. This point is further emphasized in Fig. B4. In this figure, Fig. 3 is repeated except that the conditions that $b_1 = 0$ is replaced by $b_1 = 0.2b$. Again, the relationship between Figs. 2 and 3 are similar to those between Figs. B3 and B4.

Another variation on the theme deals with a change in the normalized wavenumber (k) from the standard value of zero in Fig. 2 to the value of $(\omega\sqrt{3}/2)$ in Fig. B5. The latter value of (k) defines the components on the interface with the top fluid (fluid no. 1) that are destined to radiate into an angle (θ) of (60°) to the normal to the plane of the plate. The normalized critical frequency (ω_c), which now plays a role, is set at the standard value of ten (10) in both figures. [cf. The expression for the normalized surface impedance of the plate stated in Eq. (9)]. The influence of the plate switching from a mass control to a stiffness control surface impedance, within the range of (ω) depicted in the figures, is clearly visible in Fig. B5. In Fig. 2 that switch never occurs. Once again, this feature in the transfer function is of little significance to the arguments pursued in this paper.

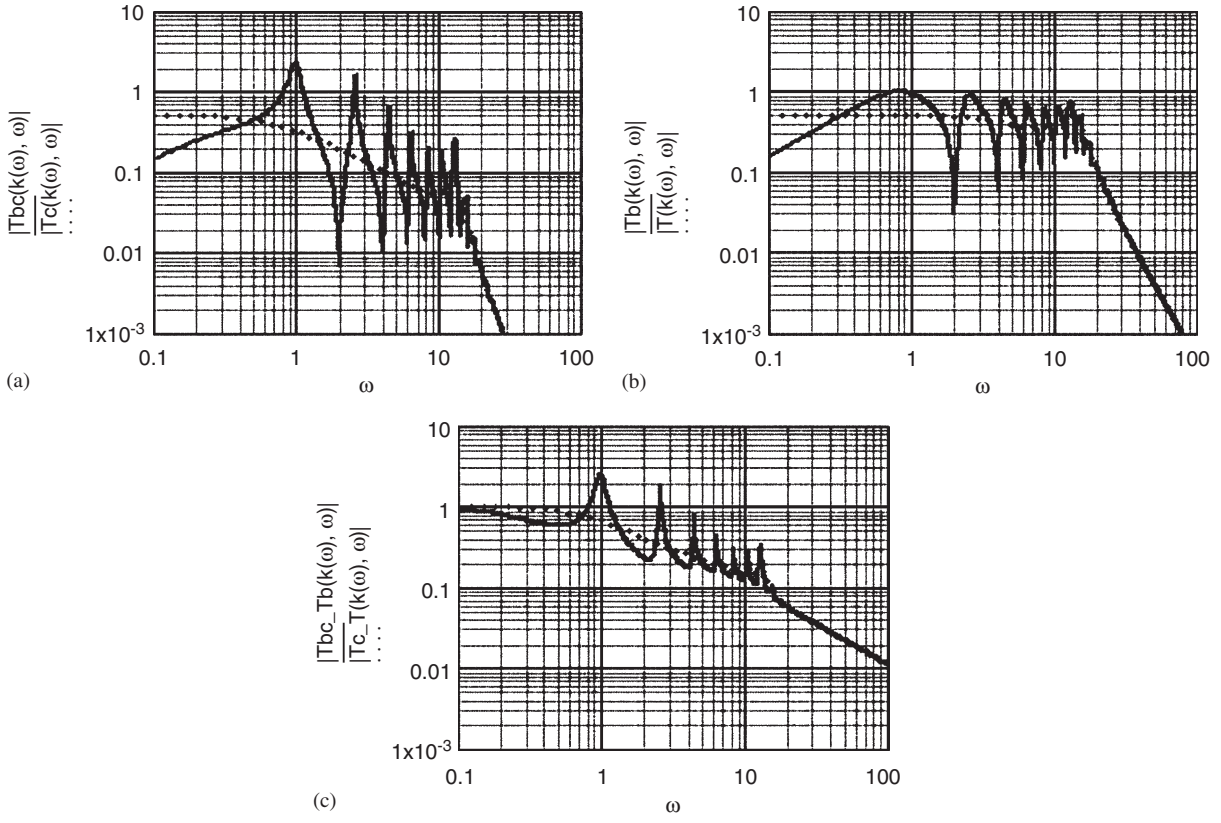

Fig. B5. The same as Fig. 2 except that the value of (k) is changed from the standard value of zero to $(\omega\sqrt{3}/2)$. Note that (k) is a normalized quantity.

It is deduced from Eq. (17a) that the modal overlap parameter $B_e(\omega)$ is dependent on the product of the effective loss factor $\eta_e(\omega)$ and the modal density $\mathrm{n}(\omega)$. Increases in $B_e(\omega)$ can thus be induced by increases in either $\eta_e(\omega), \mathrm{n}(\omega)$ or both. This property of the modal overlap parameter is central to the discussion initiating Section 4. In preceding figures changes in $B_e(\omega)$ are introduced by changes in $\eta_e(\omega)$ only. In Fig. B6 a change in the modal overlap parameter is introduced also by a change in the modal density. In this figure the normalized width (b) of the cavity is rendered dependent on the normalized frequency (ω). Instead of the standard value of $(b) = \pi$ in Fig. 2, (b) is changed to the value of $(2\pi/\sqrt{\omega})$ in Fig. B6 and, in particular, the speeds in the fluids remain equal; $c_1 = C_2$. Clearly, Fig. 2 differs from Fig. B6 in that the modal density of the resonances (and of the anti-resonances) is changed from that of

$$\mathrm{n}(\omega) = (k_2) \equiv [\cos(\theta)], \quad (b) = \pi \tag{B.1a}$$

in Fig. 2 to that of

$$\mathrm{n}(\omega) = [\cos(\theta)](\omega)^{-(1/2)}, \quad (b) = 2\pi(\omega)^{-(1/2)} \tag{B.1b}$$

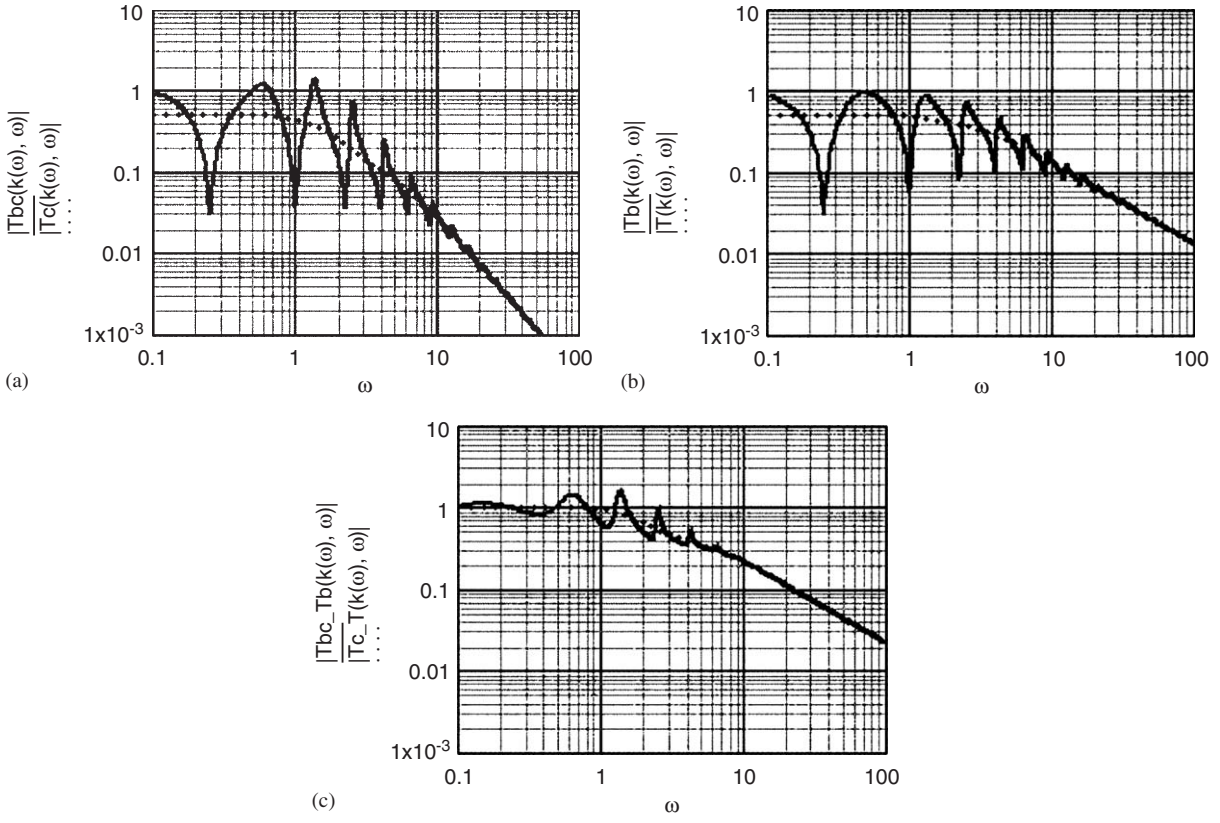

Fig. B6. The same as Fig. 2 except that the value of (b) is changed from the standard value of (π) to $(2\pi/\sqrt{\omega})$. [cf. Note that (b) and (ω) are normalized quantities and that in this figure (b) is made dependent on the normalized frequency.]

in Fig. B6. Similarly, in Fig. 2 the *modal overlap parameters* (B_b) and (B_o) are

$$B_b = (r_b/2\pi), \quad B_o = (\omega\eta)[\cos(\theta)], \tag{B.2}$$

respectively [cf. Eq. (A.8)]. In Fig. B6 these parameters change to read

$$B_b = [(r_b/2\pi)(1/2)], \quad B_o = [(\omega)^{1/2}\eta][\cos(\theta)], \tag{B.3}$$

respectively. Since (r_b) is small; $r_b = 10^{-3}$, in both, Figs. 2 and B6, (B_b) plays a minor role in these figures. Then only the change in (B_o) is significant; in Fig. 2 (B_o) is proportional to the normalized frequency (ω) and in Fig. B6 (B_o) is proportional to the square root of the normalized frequency $(\omega)^{1/2}$. Thus, $B_o(\omega)$ is lower in the higher frequency range in Fig. B6 than in Fig. 2. This difference is significant to the arguments conducted in this paper. Nonetheless, Fig. B6 is relegated to this appendix because of its physical artificiality. Of course, the bottom fluid could be made to possess a sound speed that is dispersive; e.g., $c_2 = \alpha\sqrt{\omega}$ with α a constant, but, then, too many modifications to the formalism would be required. And that too lies outside the scope of this paper.

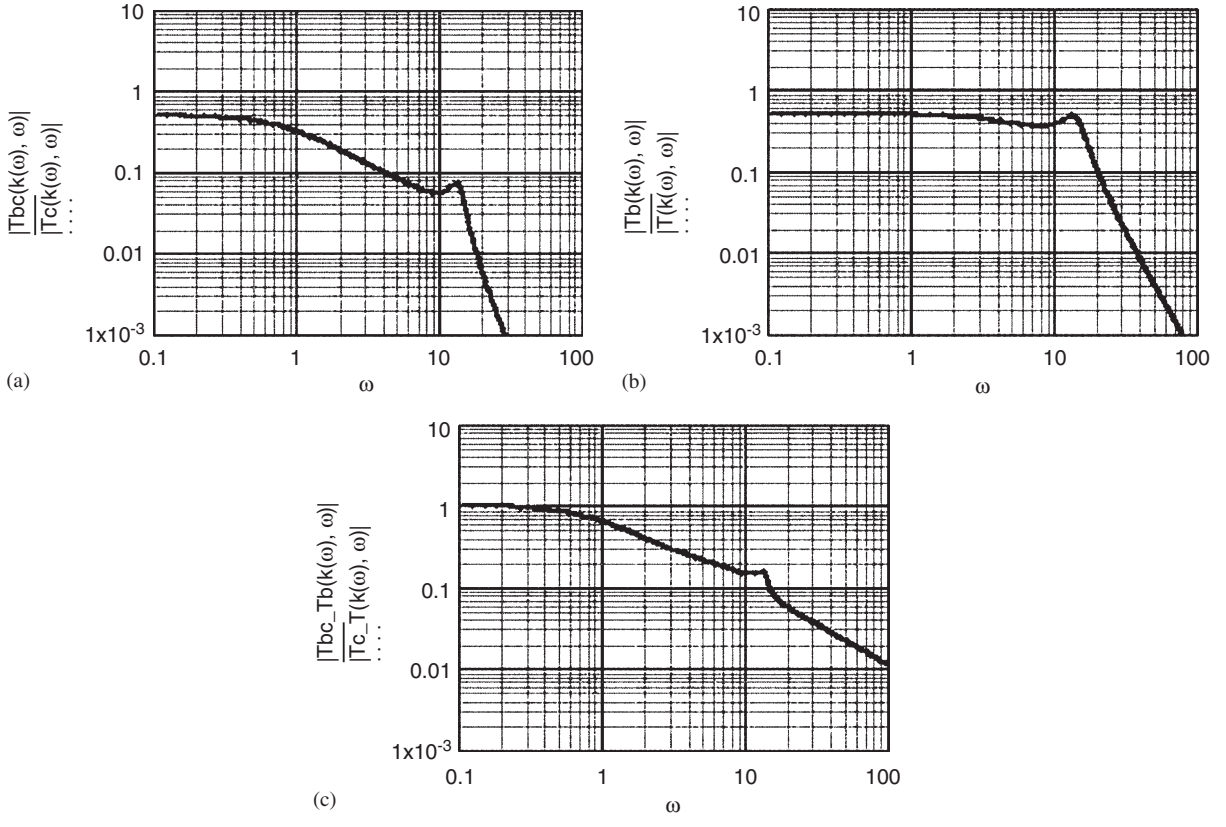

Fig. B7. The same as Fig. 9 except that the value of (k) is changed from the standard value of zero to ($\omega\sqrt{3}/2$) [cf. Fig. B5].

Last, but not least, one may wonder whether the replacement of summations by integrations can handle a change in the external sources. In Fig. 9, $s = 1$. A change in (s) from one (1) to zero (0) has been made and Fig. 9 emerged in this computation. It would be superfluous to show the result of this computation under a separate cover. And just to be clever, Fig. 9 is repeated in Fig. B7 except that the conditions on (k) are made to fit that used in Fig. B5; i.e., (k) is changed from zero to ($\omega\sqrt{3}/2$). The change in the surface impedance of the plate is clearly visible in Fig. B7 as it is in Fig. B5.

Incidentally, it may be prudent to note that the influence of the coating remains intact to changes in (s) and in (b_1). This is made clear by comparing the solid curve in Fig. 2c with the solid curves in Figs. B1(c) and B3(c) and the solid curve in Fig. 3c with the solid curves in Figs. B2(c) and B4(c), respectively.

References

[1] A. Carcaterra, A. Akay, Transient energy exchange between a primary structure and a set of oscillators: return time and apparent damping, *Journal of the Acoustical Society of America* 115 (2004) 683–696.
[2] G. Maidanik, Induced damping by a nearly continuous distribution of nearly undamped oscillators: linear analysis, *Journal of Sound and Vibration* 240 (2000) 717–731.
[3] M. Strasberg, D. Feit, Vibration of large structures by attached small resonant structures, *Journal of the Acoustical Society of America* 99 (1996) 335–344.
[4] A. Pierce, V.W. Sparrow, D.A. Russell, Fundamental structural-acoustic idealizations for structures with fuzzy internals, *Journal of Sound and Vibration* 117 (1995) 339–348.
[5] R.J. Nagem, I. Veljkovic, G. Sandri, Vibration damping by a continuous distribution of undamped oscillators, *Journal of Sound and Vibration* 207 (1977) 429–434.
[6] Yu.A. Kobelev, Absorption of sound waves in a thin layer, *Soviet Physics Acoustics* 33 (1987) 295–296.
[7] G. Maidanik, K.J. Becker, Induced noise control, *Journal of Sound and Vibration* 277 (2004) 1041–1058.
[8] M. Strasberg, Continuous structures as 'fuzzy' Substructures, *Journal of the Acoustical Society of America* 100 (1996) 3456–3459.
[9] R.H. Lyon, *Statistical Energy Analysis of Dynamic Systems: Theory and Applications*, MIT, Publication, Cambridge, 1975.
[10] R.H. Lyon, R.G. Dejung, *Theory and Application of Statistical Energy Analysis*, Butterworth-Heinemann, Publication, Boston, 1995.
[11] E. Skudrzyk, The mean-value method of predicting the dynamic response of complex vibrations, *Journal of the Acoustical Society of America* 67 (1980) 1105–1135.
[12] M.J. Brennan, Wideband vibration neutralizer, *Noise Control Engineering Journal* 45 (1997) 201–207.
[13] G. Maidanik, K.J. Becker, Criteria for designing multiple-sprung masses for wideband noise control, *Journal of the Acoustical Society of America* 106 (1999) 3119–3127.